

Entangled photons for competitive multi-armed bandit problem: achievement of maximum social reward, equality, and deception prevention

Makoto Naruse,^{1,2*} Nicolas Chauvet,² David Jegouso,² Benoît Boulanger,²

Hayato Saigo,³ Kazuya Okamura,⁴ Hirokazu Hori,⁵ Aurélien Drezet,²

Serge Huant,² Guillaume Bachelier²

¹ Network System Research Institute, National Institute of Information and Communications Technology, 4-2-1 Nukui-kita, Koganei, Tokyo 184-8795, Japan

² University Grenoble Alpes, CNRS, Grenoble INP, Institut Néel, 38000 Grenoble, France

³ Nagahama Institute of Bio-Science and Technology, 1266 Tamura, Nagahama, Shiga 526-0829, Japan

⁴ Graduate School of Informatics, Nagoya University, Furo, Chikusa, Nagoya, Aichi 464-8601, Japan

⁵ Interdisciplinary Graduate School, University of Yamanashi, Takeda, Kofu, Yamanashi 400-8510, Japan

* naruse@nict.go.jp

ABSTRACT

The competitive multi-armed bandit (CMAB) problem is related to social issues such as maximizing total social benefits while preserving equality among individuals by overcoming conflicts between individual decisions, which could seriously decrease social benefits. The study described herein provides experimental evidence that entangled photons physically resolve the CMAB, maximizing the social rewards while ensuring equality. Moreover, by exploiting the requirement that entangled photons share a common polarization basis, we demonstrated that deception, or delaying the other player receiving a greater reward, cannot be accomplished in a polarization-entangled-photon-based system, while deception is achievable in systems based on classical or polarization-correlated photons. Autonomous alignment schemes for polarization bases were also experimentally demonstrated based on decision conflict information. This study provides the foundation for collective decision making based on polarization-entangled photons and their polarization and value alignment, which is essential for utilizing quantum light for intelligent functionalities.

1. Introduction

Unique physical attributes of photons have been intensively studied for information processing to solve computationally demanding problems such as time-series prediction based on photonic reservoir computing [1], combinatorial optimization based on coherent Ising machines [2], and deep learning based on nanophotonic circuits for cognition [3]. Decision making, also called reinforcement learning, is another important branch of research where the objective is to identify decisions that will maximize benefits in dynamically changing uncertain environments [4, 5]. We previously successfully solved the multi-armed bandit (MAB) problem, which is a fundamental problem in decision making and is introduced briefly below, by employing excitation transfer via near-field coupling [6], single photons [7, 8], and chaotic lasers [9]. Meanwhile, quantum entanglement has evolved into a primary technique in quantum information processing and quantum computing [10, 11]. A fundamental question asked in the study described herein was whether quantum entanglement could have implications for reinforcement learning applications [12] or resolving the difficulties of the MAB problem.

This paper theoretically and experimentally demonstrates the usefulness and superiority of quantum-entangled photons for collective decision making or solving the MAB problem on the *social level*, for example, maximizing the total benefits while preserving equality among individuals by overcoming conflicts between individual decisions, which could seriously decrease social benefits. Moreover, by exploiting the requirement that entangled photons share a polarization basis, we demonstrate that deception, or greedily delaying the other player receiving a greater reward, is

impossible in a polarization-entangled-photon-based system, while such greedy action is achievable in systems based on classical or polarization-correlated photons. Autonomous alignment schemes for polarization bases are also experimentally demonstrated based on decision conflict information.

The MAB problem is one of the important fundamental problems in decision making, where the objective is to maximize the rewards obtained from multiple slot machines, whose reward probabilities are unknown [4]. To solve the MAB problem, it is necessary to explore better slot machines. However, too much exploration may result in excessive loss, whereas too quick of a decision or insufficient exploration may lead to missing the best machine. In our former studies, we demonstrated that the physical attributes of excitation transfer via near-field coupling, single photons, or chaotic oscillatory dynamics of semiconductor lasers can nicely solve the two-armed [6, 7, 9] and four-armed [8] bandit problems (figure 1(a)).

This type of decision-making problem becomes even more difficult when the number of decision makers, i.e. the number of individuals playing the slot machines, is multiple; then the problem is referred to as a *competitive multi-armed bandit* (CMAB) problem [13, 14], which was the focus of the study described herein. In collective decision making, social values are highlighted, such as the maximization of the total social benefits, guarantee equality among individuals, and so on [13–16]. The CMAB problem is important in practical applications ranging from traffic control, where everyone choosing the same road may lead to a traffic jam [17], to resource allocation in infrastructures, such as communications [13, 18] where everyone wanting to communicate leads to congestion for example.

We discuss a simple case in which there are two slot machines as well as two players. It is assumed that a slot machine dispenses a fixed reward for a single play even when multiple players choose that same machine. Then everyone wants more rewards and tries to select the higher-reward-probability slot machine. Eventually, the two players make the same decision, causing conflict between their decisions. In that case, the reward is divided into two halves, which are allocated to the two players (figure 1(b)). From the viewpoint that the two individuals playing the casino act as a *team*, when a player chooses the best slot machine, the other one should select the *other* machine to maximize the sum of their rewards. This example manifests itself as players easily becoming locked in a local minimum due to conflict between their decisions, whereas the total team rewards could be increased if they cooperated [13, 19].

In this study, we theoretically and experimentally demonstrated that maximally entangled photons physically resolve the CMAB problem where two players try to maximize the rewards from two slot machines. We generated entangled photon pairs using a crystal exhibiting second-order nonlinear optical properties, the signal and idler photons corresponding separately to the decisions of the two players. Photon entanglement enables conflicts between decisions to be avoided; hence, the total rewards can reach the theoretical maximum. Also, both players have equal opportunities to select the higher-reward-probability slot machine regardless of the common polarization basis; in other words, *equality* is guaranteed. In contrast, we showed that two non-cooperative players based on single-photon decision makers [7] adaptively make decisions to choose the higher-reward-probability

slot machine; however, the total reward is very limited due to the interest conflict. A better alternative is provided by polarization-correlated photon pairs [20], which enables conflicts to be avoided, although not perfectly in certain polarization configurations; however, the equality in this case is seriously decreased (see [sections 2 and 3](#)).

One important condition for collective decision making using polarization-entangled photons is that the polarization basis should be aligned among players. This requirement implies that additional functionalities are provided by polarization-entangled photons in decision making and indicates the importance of autonomous polarization alignment mechanisms for robust system operation. In this report, we demonstrated that deception, or delaying the other player from receiving a greater reward, is impossible if polarization-entangled-photon-based decision making is employed, while deception is achievable in systems based on classical or polarization-correlated photons (see [section 4](#)). Moreover, the experimental demonstration of autonomous online alignment schemes for polarization bases using information about decision conflicts is described (see [section 5](#)).

The usefulness of entangled photons is addressed in the quantum game literature [21–24] regarding resolving Nash equilibrium in non-cooperative games formulated by payoff matrices in game theory [25]. The study described herein was focused on the CMAB problem, which differs from the non-zero-sum game [22] in the sense that the reward in the CMAB problem is not given deterministically, unlike in conventional game theory, but rather probabilistically; thus, one can *lose* even when the choice is *correct*, and vice versa. Hence, it is not possible to address the CMAB problem

using the payoff matrix formulation alone. The objective of the CMAB problem is completely different from that of the zero-sum game [24]: it is not desirable for one player to beat the other by using quantum protocols. Instead, equality and maximal total reward or social gain are demanded, which are of utmost importance for allocating resources according to the CMAB problem formulation. Consequently, inhibition of greedy players, and affirmative action for handicapped players in some cases, is an important concern. In this report, we highlight the usefulness of a shared polarization basis for polarization-entangled photons, i.e. the signal and idler photons, from the viewpoint of such novel social figures. Indeed, a detailed analysis of the polarization basis, which is also necessary for quantum games, has not been provided elsewhere. Likewise, dynamic operations are necessary for CMAB applications. We also demonstrate autonomous polarization alignment schemes for robust system operation.

2. Principle and theory

2.1. System architecture

For the simplest case that preserves the essence of the CMAB problem, we considered two players called Players 1 and 2 hereafter, each of whom selected one of two slot machines (Machines A and B hereafter), with the goal of maximizing the total social reward. The reward probabilities of Machines A and B are denoted as P_A and P_B , respectively. The amount of reward that could be dispensed by each slot machine per play was assumed to be unity.

An overview of the experimental setup used to generate and analyse the photon states for selecting Machine A or Machine B is provided in [figure 2](#), and its details are described in [Appendix A](#). The output of the excitation laser passed through a polarizer, half-wave plate (denoted HW_E), quarter-wave plate (QW_E), and dichromic mirror (D), and it was incident upon a polarization beam splitter (PBS_L). The horizontally and vertically polarized components of the incoming light travelled clockwise and anti-clockwise, respectively, through a Sagnac loop containing a half-wave plate (HW_L) and type II quasi-phase-matched periodically poled KTiOPO_4 (PPKTP) nonlinear crystal (Cr), where spontaneous parametric down conversion (SPDC) was induced [26]. The entanglement of orthogonally polarized photons was generated in the PBS_L , where the two paths were recombined [27]. The signal and idler photons corresponded to the outgoing components from the PBS_L ; the signal photons were directed into the branch for the decision making of Player 1, whereas the idler photons travelled to the branch for the decision making of Player 2 [27]. Note that the signal and idler photons had distinct wavelengths and were spectrally selected to avoid contamination, which would have affected the final choices of the players (see [Appendix A](#) for details).

For entangled photon generation, it was necessary for HW_E and QW_E to be installed properly to satisfy the condition of generating SPDC equally through both optical paths of the Sagnac loop. Thus, *classical*, which means not entangled, *polarization-correlated* photon pairs could also be generated easily by orienting the wave plates so that only the horizontally or vertically polarized component of the excitation laser was incident and travelled through the Sagnac loop either clockwise

or anti-clockwise. The precise definition of polarization-correlated photons in this study is given later on. In addition to the benefits of the superior stability of generating SPDC by the Sagnac loop system [27], the difference between polarization-correlated and polarization-entangled photon pairs could easily be investigated using the same experimental architecture.

In the branch corresponding to Player 1, each signal photon went through another half-wave plate (HW_1), and was subjected to a PBS (PBS_1). If the photon was detected by the avalanche photodiode corresponding to the horizontally polarized light (APD1), the decision of Player 1 was to choose Machine A, whereas if the photon was detected by the avalanche photodiode corresponding to the vertically polarized light (APD2), then the decision of Player 1 was to choose Machine B.

Likewise, in the branch corresponding to Player 2, each idler photon went through another half-wave plate (HW_2) and was subjected to a PBS (PBS_2). If the photon was detected by the avalanche photodiode corresponding to the horizontally polarized light (APD3), then the decision of Player 2 was to choose Machine A, whereas if the photon was detected by the avalanche photodiode corresponding to the vertically polarized light (APD4), then the decision of Player 2 was to choose Machine B.

Note that the two slot machines were externally arranged in the experiment, and we emulated the slot machines in a computer using pseudorandom sequences (see [Appendix A](#) for details).

2.2. Decision making by a *single* player

We started with the *single*-player situation, in which either Player 1 or Player 2 attacked, which is essentially equivalent to that whose experimental demonstration is described in [7]. In this case, it is desirable for the player to choose higher-reward-probability slot machine, since a larger reward is desired. With linearly polarized single photons, the idea of a single-photon-based decision maker [7] is to rotate the half-wave plate (HW₁ or HW₂), so that more photons are detected by the channel corresponding to the higher-reward-probability slot machine.

For later use, we now introduce several types of notation employed to describe the system. The input photon state (polarization angle) for the decision making of Player i ($i = 1, 2$) is denoted as $|\theta_i\rangle$, while the angle of HW _{i} is denoted as θ_{HW_i} . The roles of HW _{i} and PBS _{i} are given respectively by

$$HW_i|\theta_i\rangle = |2\theta_{\text{HW}_i} - \theta_i\rangle \quad (1)$$

and

$$PBS_i|2\theta_{\text{HW}_i} - \theta_i\rangle = \cos(2\theta_{\text{HW}_i} - \theta_i)|H_i\rangle + \sin(2\theta_{\text{HW}_i} - \theta_i)|V_i\rangle, \quad (2)$$

where $|H_i\rangle$ and $|V_i\rangle$ indicate the polarization bases of PBS _{i} [28]. Therefore, the probabilities of photon measurement by APD1 and APD2, for example, which determined whether Player 1 decided to select Machine A or Machine B, were given by $\cos^2(2\theta_{\text{HW}_1} - \theta_1)$ and $\sin^2(2\theta_{\text{HW}_1} - \theta_1)$, respectively. Using the tug-of-war principle described in [7], which is also summarized in the Methods section, the wave plate angle was controlled toward the higher-reward-probability slot machine.

In the *single*-player decision-making experiment, the nonlinear crystal was excited in one of the Sagnac loops, so that no entanglement could occur. In addition, we inserted polarizers in front of

the half-wave plates, marked P* in [figure 2](#), to configure $|\theta_i\rangle = |\pi/4\rangle$ for both players ($i = 1, 2$). The experimental details are described in [section 3](#).

2.3. Decision making by *non-cooperative* players

Then we considered a situation in which *both* Players 1 and 2 were completely independent and simultaneously chose the slot machines, as shown in [figure 1\(b\)](#). Thus, they played the slot machines in a non-cooperative manner. Following the strategy described above, both Players 1 and 2 tried to select the higher-reward-probability slot machine, leading to conflict between their decisions. If the slot machine dispensed a reward, each player could only receive a *half* reward. In terms of reward, this penalty was intended to favour collective, i.e. not conflictual, choices with respect to individual interests.

2.4. Decision making by *polarization-correlated* photons

Toward realizing collective decision making, two conditions must be fulfilled. The first method of avoiding conflicts between decisions was to introduce correlations between the two photons, thereby statistically linking the decisions of Players 1 and 2. To this end, we used polarization-orthogonal photon pairs denoted by $|\theta_1, \theta_2\rangle$, where

$$\theta_2 = \theta_1 + \pi/2. \tag{3}$$

The underlying idea of using orthogonal polarizations was to promote the players to select distinct machines. Each photon then encountered a polarization rotation and polarization beam splitter, represented by [equations \(1\) and \(2\)](#). Finally, the probability amplitudes of observing photons at one of APD1 and APD2, *and* at one of APD3 and APD4 were as follows:

$$[\text{APD1 and APD3}] \langle H_1, H_2 | M | \theta_1, \theta_2 \rangle = \cos(2\theta_{\text{HW}_1} - \theta_1) \cos(2\theta_{\text{HW}_2} - \theta_2), \quad (4)$$

$$[\text{APD1 and APD4}] \langle H_1, V_2 | M | \theta_1, \theta_2 \rangle = \cos(2\theta_{\text{HW}_1} - \theta_1) \sin(2\theta_{\text{HW}_2} - \theta_2), \quad (5)$$

$$[\text{APD2 and APD3}] \langle V_1, H_2 | M | \theta_1, \theta_2 \rangle = \sin(2\theta_{\text{HW}_1} - \theta_1) \cos(2\theta_{\text{HW}_2} - \theta_2), \quad (6)$$

and

$$[\text{APD2 and APD4}] \langle V_1, V_2 | M | \theta_1, \theta_2 \rangle = \sin(2\theta_{\text{HW}_1} - \theta_1) \sin(2\theta_{\text{HW}_2} - \theta_2), \quad (7)$$

where M denotes operators consisting of wave plates and polarization beam splitters. The coincidence of observing photons at APD1 and APD3, and at APD2 and APD4 according to [equations \(4\) and \(7\)](#) respectively indicates conflict between the decisions made by Players 1 and 2.

Correlated photon polarization is not a sufficient condition to prevent conflict: in view of both players acting as a team, they must also perform coherent choices. This insufficiency led to the second requirement, namely, the use of correlated wave plate angles. Here, we represent this condition by the rotation of both wave plates by the same amount; that is:

$$\theta_{\text{HW}_2} = \theta_{\text{HW}_1}. \quad (8)$$

By subjecting [equations \(3\) and \(8\)](#) to [equations \(4\) to \(7\)](#), the probability of conflict between decisions is

$$P_C = \frac{1}{4} \left[1 - \cos(8\theta_{\text{HW}_1} - 4\theta_1) \right], \quad (9)$$

which can be obtained by summing the squared moduli of [equations \(4\)](#) and [\(7\)](#), while the probability of *no* conflict between decisions is:

$$P_{NC} = 1 - P_C = \frac{1}{4} \left[3 + \cos(8\theta_{\text{HW}_1} - 4\theta_1) \right]. \quad (10)$$

From [equation \(9\)](#), θ_{HW_1} should be configured as $\frac{\theta_1}{8} + \frac{\pi}{4} \times N$, with N being a natural integer to avoid conflict between decisions. Note that it is technically impossible if the photon state θ randomly varies from photon to photon. Furthermore, even when conflict between decisions is successfully avoided, i.e. by using fixed θ , the resulting decision is *biased* toward a specific machine, leading to a reward distribution that is biased toward a specific player. It means that the *equality* between the players decreases.

Using polarization-correlated photon pairs characterized by [equations \(4\) – \(7\)](#), the expected reward received by Player 1 in a single play is

$$\begin{aligned} E[R_1] = & P_A \times \cos^2(2\theta_{\text{HW}_1} - \theta_1) \sin^2(2\theta_{\text{HW}_1} - \theta_1) + P_A \times \cos^2(2\theta_{\text{HW}_2} - \theta_1) \cos^2(2\theta_{\text{HW}_2} - \theta_1) \times 0.5 \\ & + P_B \times \sin^2(2\theta_{\text{HW}_1} - \theta_1) \sin^2(2\theta_{\text{HW}_2} - \theta_1) \times 0.5 + P_B \times \cos^2(2\theta_{\text{HW}_2} - \theta_1) \sin^2(2\theta_{\text{HW}_1} - \theta_1), \end{aligned} \quad (11)$$

which can be reduced to

$$\begin{aligned} E[R_1] = & 0.375(P_A + P_B) + 0.0625(P_A + P_B) \cos[4(\theta_{\text{HW}_1} - \theta_{\text{HW}_2})] \\ & + 0.0625(P_A + P_B) \cos[4(\theta_{\text{HW}_1} - \theta_{\text{HW}_2} - \theta_1)] \\ & + 0.375(P_A - P_B) \cos(4\theta_{\text{HW}_1} - 2\theta_1) + 0.125(P_A - P_B) \cos(4\theta_{\text{HW}_1} - 2\theta_1) \end{aligned} \quad (12)$$

Likewise, the expected reward received by Player 2 is

$$\begin{aligned}
E[R_2] = & 0.375(P_A + P_B) + 0.0625(P_A + P_B)\cos[4(\theta_{HW_1} - \theta_{HW_2})] \\
& + 0.0625(P_A + P_B)\cos[4(\theta_{HW_1} - \theta_{HW_2} - \theta_1)] \\
& + 0.375(P_B - P_A)\cos(4\theta_{HW_1} - 2\theta_1) + 0.125(P_B - P_A)\cos(4\theta_{HW_1} - 2\theta_1)
\end{aligned} \tag{13}$$

From equations (13) and (12), the expected amount by which the reward of Player 2 exceeds that of Player 1 is given by:

$$E[R_2] - E[R_1] = \frac{1}{2}(P_B - P_A)[\cos(4\theta_{HW_1} - 2\theta_1) + \cos(4\theta_{HW_2} - 2\theta_1)]. \tag{14}$$

It means that the expected reward could be biased toward a particular player depending on the difference between the polarization bases and the incoming photon polarization. In addition, this characteristic implies that no matter what θ_1 and θ_{HW_1} are, it is *possible* for Player 2 to receive a reward greater than (or at least equal to) that received by Player 1 by configuring

$$\theta_{HW_2} = \frac{1}{2}\theta_1 + \frac{N\pi}{2}, \tag{15}$$

where N is a natural integer. Thus, *deception*, or greedy action by a player in the system to gain a greater reward than the other, is generally *achievable* when the system is governed by correlated photons. The red circles and blue squares in figure 3(a) represent some of the expected rewards of Players 1 and 2, assuming that $\theta_{HW_1} = 0^\circ$, θ_1 ranges from 0° to 180° , and P_A and P_B are 0.2 and 0.8, respectively. Clearly, Player 2 can succeed in maximally deceiving (or at least receiving a reward equal to that of) Player 1 by choosing θ_{HW_2} according to equation (15).

2.5. Decision making using *polarization-entangled* photons

To avoid conflict between decisions, the probability amplitudes in equations (4) and (7) must always vanish, requiring a second contribution exactly cancelling the oscillating sine and cosine terms. To this end, we utilized a coherent superposition of states made of entangled states. As described in section 1, the signal and idler photons were employed for the decisions of Players 1 and 2, respectively. Due to the symmetry of the equations, a natural choice was to exchange the roles of θ_1 and θ_2 and to introduce a phase shift of π , or, in other words, to use a specific entangled state known as the maximally entangled singlet photon state and given by

$$\frac{1}{\sqrt{2}}(|\theta_1, \theta_2\rangle - |\theta_2, \theta_1\rangle), \quad (16)$$

where θ_1 and θ_2 are orthogonal to each other as specified in equation (3). The probability amplitude originating from the *second* term of equation (16) can be derived according to the following equations:

$$[\text{APD1 and APD3}] - \langle H_1, H_2 | M | \theta_2, \theta_1 \rangle = -\cos(2\theta_{\text{HW}_1} - \theta_2) \cos(2\theta_{\text{HW}_2} - \theta_1), \quad (17)$$

$$[\text{APD1 and APD3}] - \langle H_1, V_2 | M | \theta_2, \theta_1 \rangle = -\cos(2\theta_{\text{HW}_1} - \theta_2) \sin(2\theta_{\text{HW}_2} - \theta_1), \quad (18)$$

$$[\text{APD2 and APD3}] - \langle V_1, H_2 | M | \theta_2, \theta_1 \rangle = -\sin(2\theta_{\text{HW}_1} - \theta_2) \cos(2\theta_{\text{HW}_2} - \theta_1), \quad (19)$$

and

$$[\text{APD2 and APD4}] - \langle V_1, V_2 | M | \theta_2, \theta_1 \rangle = -\sin(2\theta_{\text{HW}_1} - \theta_2) \sin(2\theta_{\text{HW}_2} - \theta_1). \quad (20)$$

Before proceeding, we remark upon the difference between *correlated* and *entangled* photons in this study. For the *correlated* photons, the photon state was *factorized*. In contrast, the states of the quantum-*entangled* photons were given by quantum superposition: they were non-separable. Actually, the correlated photons in this study were not arbitrarily factorized in view of the SPDC generation

process; the photon polarizations were always orthogonal and were not given by a photon state $|\theta_1, \theta_2\rangle$ with θ_1 and θ_2 being random from pair to pair, which is also a factorized state. The polarizations of the two photons in each pair in the present study were not arbitrary, but rather were *correlated* according to the quasi-phase-matching conditions of SPDC in the crystal.

The probability of photodetection at both APD1 and APD3, meaning that both Players 1 and 2 select Machine A, is given by the squared modulus of the *coherent* sum of [equations \(4\) and \(17\)](#), both multiplied times $1/\sqrt{2}$, which leads to:

$$P_{1\&3} = \frac{1}{2} \sin^2 \left[2(\theta_{\text{HW}_1} - \theta_{\text{HW}_2}) \right]. \quad (21)$$

This probability *always* yields zero *regardless* of the values of θ_i and θ_{HW_i} as long as the conditions of [equations \(3\) and \(8\)](#) apply. Likewise, the probability of photodetection at APD2 and APD4, meaning that both Players 1 and 2 select Machine B, is given by [equation \(16\)](#) and therefore is also *always zero*. Thus, conflicts between decisions *never* occur, leading to the maximum overall social reward.

Conversely, the probability of observing photons at APD1 and APD4 can be expressed as

$$P_{1\&4} = \frac{1}{2} \cos^2 \left[2(\theta_{\text{HW}_1} - \theta_{\text{HW}_2}) \right], \quad (22)$$

as given by the squared modulus of the coherent sum of [equations \(5\) and \(13\)](#), both multiplied times $1/\sqrt{2}$, which is *always* 0.5 when [equations \(3\) and \(8\)](#) are satisfied. Likewise, the probability of observing photons at APD2 and APD3 is given by [equation \(22\)](#). Thus, both players have equal opportunities to select each slot machine, which is the foundation of the equality provided by polarization-entangled photons.

Based on [equations \(21\)](#) and [\(22\)](#), the expected reward received by Player 1 for a single play is:

$$E[R_1] = P_A \times \frac{1}{2} \sin^2 \left[2(\theta_{\text{HW}_1} - \theta_{\text{HW}_2}) \right] + P_A \times \frac{1}{2} \cos^2 \left[2(\theta_{\text{HW}_1} - \theta_{\text{HW}_2}) \right] \times 0.5 \\ + P_B \times \frac{1}{2} \cos^2 \left[2(\theta_{\text{HW}_1} - \theta_{\text{HW}_2}) \right] \times 0.5 + P_B \times \frac{1}{2} \sin^2 \left[2(\theta_{\text{HW}_1} - \theta_{\text{HW}_2}) \right] \quad (23)$$

The multiplication times 0.5 in the second and third terms on the right-hand side indicates that the reward is reduced to half due to the conflict between decisions. [Equation \(23\)](#) can be recast as

$$E[R_1] = 0.375(P_A + P_B) + 0.125(P_A + P_B) \cos \left[4(\theta_{\text{HW}_1} - \theta_{\text{HW}_2}) \right] \quad (24)$$

The expected amount of reward received by Player 2 also results in [equation \(24\)](#). That is, no matter how Player 2 configures θ_{HW_2} , the rewards allocated to Players 1 and 2 are the same. Thus, even if Player 2 knows the higher-reward-probability machine and can rotate the wave plate with the intention of receiving a greater reward, such deception is *impossible* if the system is governed by polarization-entangled photons. Moreover, the expected total reward received by Players 1 and 2, given by 2 times [equation \(24\)](#), i.e.:

$$E[R_{\text{TEAM}}] = 0.75(P_A + P_B) + 0.25(P_A + P_B) \cos \left[4(\theta_{\text{HW}_1} - \theta_{\text{HW}_2}) \right] \quad (25)$$

is *less than* its maximum value, given by $P_A + P_B$, if the half-wave plate alignment is disrupted ($\theta_{\text{HW}_1} \neq \theta_{\text{HW}_2}$) unless $\theta_{\text{HW}_2} = \theta_{\text{HW}_1} + N \times \pi / 2$ with N being a natural integer. That is, in addition to the inhibition of deception, the total social benefits are decreased if a selfish action is performed by one of the players.

The red circles and blue squares in [figure 3\(b\)](#) represent the expected rewards of Players 1 and 2 assuming that $\theta_{\text{HW}_1} = 0^\circ$, while θ_1 ranges from 0° to 180° . Clearly, polarization-entangled photons give *equal* expected rewards for any value of θ_1 and θ_{HW_2} , and they decrease the rewards when θ_{HW_2} is different from θ_{HW_1} .

3. Experimental results: Collective decision making in the CMAB problem

3.1. Decision making by a single player

The reward probabilities of Machines A and B were $P_A = 0.2$ and $P_B = 0.8$, respectively, for the first 50 plays. In the next 50 plays, the reward probabilities were swapped, i.e. $P_A = 0.8$ and $P_B = 0.2$, to emulate a variable environment ([figure 5\(a\)](#)). Therefore, from the standpoint of *individual* players, selecting Machine B was the *correct* decision in the first 50 plays since it was highly likely to provide a greater reward. Likewise, choosing Machine A was correct for the next 50 plays.

For Player 1, the decision was to choose Machine A when the photon was observed by APD1 and Machine B when the photon was detected by APD2. [Figure 4\(a\)](#) shows the photon detection rate statistics observed in 2 s as a function of the HW_1 angle. The photon counts are nearly equal when the wave plate angle is 0° , whereas the detection rate of APD1 exceeds that of APD2 with decreasing wave plate angle; and it becomes less than that of APD2 with increasing wave plate angle. The adaptive decision making was implemented by updating the wave plate orientation toward the higher-reward-probability slot machine by revising the polarization adjuster (PA) values [\[7\]](#). The details of controlling

the PA values are described in [7] and Appendix B. In the experiment, we used seven discrete half-wave plate orientations specified by the PA values ranging from -3 to 3 to compensate for the photon count asymmetry. Correspondingly with these orientations, the ratio between the photon count by APD1 and the photon count by APD2 was 20, 10, 5, 1, $1/5$, $1/10$, and $1/20$, which effectively resolves the asymmetry.

For Player 2, the decision was to choose Machine A when the photon was observed by APD3, and to choose Machine B when the photon was detected by APD4. Figure 4(b) shows the photon detection rate statistics observed in 2 s as a function of the angle of the second half-wave plate (HW_2). Using exactly the same method as described above for Player 1, adaptive decision making was realized by updating the orientation of HW_2 .

First, only Player 1 played the casino. Specifically, Player 1 conducted 100 consecutive slot plays, and this set of plays was repeated 10 times. The red curve shown in figure 5(b, i) represents the *correct decision ratio (CDR)* defined as the ratio of the number of selections of the machine yielding a higher reward probability over the number of trials at cycle t . This ratio quickly approaches unity, meaning that Player 1 effectively chose the higher-reward-probability machine, i.e. Machine B. At cycle 51, the CDR drops due to the flip of the reward probabilities, which was done to mimic environmental uncertainty. However, the CDR gradually returns to unity as time elapses, which clearly indicates that Player 1 detected the change in the environment and revised the decision to the higher-reward-probability machine, i.e. Machine A. The red curve in figure 5(b, ii) shows the evolution of the

accumulated reward averaged over 10 repetitions, which almost linearly increases with time. Its growth is attenuated after cycle 50 due to the reward probability change. Note that the accumulated reward of Player 1 at cycle 100 is about 66.

The blue curves in [figures 5\(c, i\)](#) and [5\(c, ii\)](#) show the CDR and accumulated reward when only Player 2 played the slot machines. The behavior is similar to the case of Player 1. The accumulated reward at cycle 100 is 67, which is almost equivalent to that in the case of Player 1. This finding demonstrates the successful decision making by single players as well as the validity of the strategy adopted for solving the asymmetry between APD collection efficiencies.

3.2. Decision making by two *non-cooperative* players

Next, we discuss the case in which both Players 1 and 2 independently played the slot machines; in other words, they played in a non-cooperative manner. The red and blue curves in [figure 5\(d, i\)](#) are the CDRs of Players 1 and 2, respectively, both of which exhibiting traces similar to those in the single-player cases ([figures 5\(b\)](#) and [5\(c\)](#)). Actually, both Players 1 and 2 succeeded in finding higher-reward-probability slot machine over time. However, this result indicates conflict between their decisions; hence, the accumulated rewards of Players 1 and 2 shown by the red and blue curves, respectively, in [figure 5\(d, ii\)](#) are seriously decreased, i.e. nearly half of those in the single-player cases. The summation of the accumulated rewards of Players 1 and 2, referred to as the *team* reward, is depicted by the green curve in [figure 5\(d, ii\)](#) and is 70.9 at cycle 100, which is only slightly larger than in the

single-player cases. Indeed, the *conflict ratio*, which is defined as the number of times that the decisions of Players 1 and 2 are identical over the 10 repetitions, exhibits higher values closer to unity, as shown by the red curve in [figure 5\(d, iii\)](#). This result indicates that conflicts between decisions occurred very frequently during the slot plays.

3.3. Decision making using *polarization-correlated photons*

In the next configuration, Players 1 and 2 employed orthogonally polarized photon pairs. Experimentally, the nonlinear crystal was pumped only by a laser beam traveling anti-clockwise in the Sagnac loop thanks to the proper adjustment of HW_E and QW_E . To mimic a correlated choice in the team, the half-wave plates of Players 1 and 2, i.e. HW_1 and HW_2 , respectively, were rotated in the same manner so that the polarizations of those branches were simultaneously rotated by 0° , 15° , 30° , 45° , 60° , 75° , and 90° . Thus, seven different kinds of orthogonally polarized photons were subjected to the decision making of Players 1 and 2. Setting exactly the same conditions for the casino as in the former cases, 100 consecutive slot plays were repeated 10 times for each of the seven polarization bases. The experimental details are described in [Appendix C](#).

The red and blue curves in [figure 6\(a, i\)](#) show the CDRs of Players 1 and 2 with a polarization angle of 45° : one photon was incident upon PBS_1 with an angle of 45° with respect to the horizontal, and the other photon was incident upon PBS_1 with an angle of -45° with respect to the horizontal. The CDRs fluctuate around 0.5, meaning that both Players 1 and 2 did not necessarily select the higher-

reward-probability slot machine. The apparently large noise is simply due to averaging over 10 repetitions, giving a typical standard deviation of only $\sqrt{10}$. However, the team reward, equal to the sum of the rewards of Players 1 and 2 grows more rapidly than in the case of two non-cooperative players, reaching an accumulated reward of about 79.4 at cycle 100, as shown by the green curve in [figure 6\(a, ii\)](#). However, the conflict rate is still higher, as shown by the red curve in [figure 6\(a, iii\)](#). The reason for this result is that the event of detecting photons by $|H_1\rangle$ or $|V_1\rangle$ for Player 1 was probabilistic (50:50), and the same was true for Player 2, for photons impinging on the PBSs at $\pm 45^\circ$. Hence, conflicts between decisions could not be avoided, causing the team reward to decrease.

3.4. Decision making using *polarization-entangled photons*

Finally, maximally entangled photon pairs were employed for the decisions of Players 1 and 2. Experimentally, the nonlinear crystal was pumped by laser beams traveling both clockwise- and anti-clockwise thanks to the proper configuration of the half- and quarter-wave plates in the path of the excitation laser: HW₁ and HW₂ were rotated in the same manner as in the orthogonally polarized photon pair case described above, to preserve the coherence in the team choices. [Figure 4\(c\)](#) characterizes the optical system by presenting the coincidence rate statistics measured over 2 s regarding the joined photodetection as a function of the rotation of HW₁ and HW₂. For that we used the following sets of detectors: (i) APD1 and APD3 (downward triangles), (ii) APD1 and APD4 (circles), (iii) APD2 and APD3 (diamonds), and (iv) APD2 and APD4 (upward triangles). The large

coincidences of (ii) and (iii), and smaller coincidences of (i) and (iv) throughout the polarization basis clearly demonstrate the successful establishment of cross-polarized entangled photon pairs.

The red and blue curves in figure 6(b, i) show the CDRs of Players 1 and 2, respectively, with 45° polarization. They fluctuate around 0.5, which means that both Players 1 and 2 did not necessarily choose the higher-reward-probability slot machine, as in figure 6(a, i). In contrast, the team reward shown by the green curve in figure 6(a, ii) grows more rapidly than in the case of two correlated-photon-pair-driven players: it reaches an accumulated reward of about 93.4 at cycle 100, which is approaching the theoretical maximum of the total reward. The theoretical maximum of the average team reward is $(P_A + P_B) \times 100 = 100$. The conflict rate in the case of entangled-photon-based decisions is shown by the red curve in figure 6(b, iii), and remains low. This finding is consistent with the greater team reward mentioned above. The non-zero value is due to imperfections in the experimental setup.

3.5. Comparison of decision-making strategies

Figures 6(c) and 6(d) characterize the details of the collective decision-making performance with respect to the polarization basis. Figures 6(c, i) and 6(d, i) depict the accumulated reward at cycle 100 as a function of the common orientation of the half-wave plates, which corresponds to the polarization basis, regarding the decision making based on polarization-correlated and polarization-entangled photon pairs, respectively. The red squares, blue diamonds, and green circles correspond to the rewards received by Player 1, Player 2, and the team, respectively.

The team reward is very high, about 100, when the polarization is 0° and 90° , even in the case of correlated photon pairs. For example, a correlated photon pair given by $|H_1, V_2\rangle$ is a photon pair corresponding to the polarization angle $\theta_1 = 0^\circ$. In this case, Player 1 always detects an $|H_1\rangle$ photon, leading to the decision to choose Machine A, whereas Player 2 always detects a $|V_2\rangle$ photon. It indicates that the decision is to select Machine B. Therefore, from the viewpoint of *correct* decision making, Player 2 achieves a higher CDR in the first 50 cycles and a lower CDR in the second 50 cycles due to the reward probability flipping, as clearly demonstrated in [figure 6\(c, ii\)](#)[0]. A similar tendency is observable with the input photon pair described by $|V_1, H_2\rangle$ that corresponds to the polarization angle $\theta_1 = 90^\circ$, as shown in [figure 6\(c, ii\)](#)[90]. The conflict ratio remains lower in these specific polarization cases than others, as shown by the red squares in [figure 6\(c, iii\)](#).

However, in terms of *equality* (or *fairness*) this scenario is highly inefficient since a player can select either machine. Indeed, with 0° polarization, only Player 2 earns a greater reward in the first 50 plays, and the imbalance between Players 1 and 2 is significant. More specifically, the equality depicted by the diamonds in [figure 6\(c, iii\)](#) is significantly decreased; it is defined as the average ratio between the numbers of times that the higher-reward-probability machine was selected by Players 1 and 2. The exact definition of equality is provided in [Appendix D](#).

On the contrary, with the use of entangled photons, the team reward always reaches the theoretical maximum (100) regardless of the polarization basis, as shown in [figure 6\(d, i\)](#). It is due to the maximally entangled state that is invariant upon rotation of the basis, provided that the bases are

the same for both players. The CDRs of Players 1 and 2 always randomly fluctuate around 0.5, as shown in [figure 6\(d, ii\)](#). This fluctuation agrees with the fact that nearly identical rewards were received by Players 1 and 2, as can be seen in [figure 6\(d, i\)](#). The conflict rate, shown by the red squares in [figure 6\(d, iii\)](#), is always small regardless of the polarization basis. Finally, the equality remains always high for all of the polarization bases, clearly showing that the entangled states yielded results superior to those achievable using the correlated states in terms of all of the investigated social properties.

To summarize the figures of merit of all of the decision-making strategies, the total rewards resulting from using single-photon decision making for single players and non-cooperative and collective decision making are compared in [figure 7\(a\)](#). The orange and green bars depict the experimental and simulation results, respectively, which agree well throughout the experiments. For the two-player games, the experimentally obtained rewards of the individual players are also shown: red for Player 1 and purple for Player 2. The diagonal and vertical stripes areas indicate the rewards accumulated during the first 50 and second 50 plays, respectively, emphasizing the effective equality or inequality between the two players. The error bars show the maximum and minimum observed values.

Clearly, the maximum team reward was achieved by using entangled photons. Furthermore, the individual rewards in the entangled photon case are higher than those in the case of two non-cooperative players, indicating that non-conflict and equal opportunities not only lead to the social maximum, but also benefit the individual players.

In the next step, we changed the reward probabilities of the slot machines: $P_A = 0.4$ and $P_B = 0.6$ were used for the first 50 cycles, followed by $P_A = 0.6$ and $P_B = 0.4$ for the second 50 cycles. It appeared that finding the higher-reward-probability machine was more difficult in that case due to the difference between the reward probabilities being smaller than in the former cases. The blue bars in [figure 7\(b\)](#) show the accumulated rewards at cycle 100 for all of the cases. Indeed, for Player 1 only, Player 2 only, and two non-cooperative players, the total reward is substantially lower than in the former cases depicted by the red bars. These differences are due to the longer time needed to reach stable selection of the higher-reward-probability machine. On the contrary, with correlated and entangled photons, the team reward does not change, and the entangled photons again provide the maximum total reward. This finding clearly demonstrates that collective decision making based on entangled photons ensures that the social maximum reward will be achieved regardless of the difficulty of the given problem.

4. Experimental results: Deception or greedy action

An important condition for establishing the social maximum in the CMAB solution by using polarization-entangled photons is sharing of the polarization basis among the players. By exploiting this property, we theoretically showed in [sections 2.4](#) and [2.5](#) that polarization-entangled photons inhibit deception or delaying the other player receiving a greater reward, whereas correlated photons do allow such greedy actions. This section describes the corresponding experimental demonstrations.

4.1. Decision making in *polarization-entangled-photon-based* systems

We investigated a scenario in which one of the players was *greedy*, and tried to *deceive* the other player to obtain a greater reward. It was assumed that Player 2 started such greedy actions by using the single-photon decision-making strategy demonstrated in [section 2.2](#) [7, 8]: for that the half-wave plate has to be rotated by θ_{HW_i} in the direction of the higher-reward-probability machine.

The casino setting was configured in the same way as in the cases discussed in [section 3](#): the reward probabilities of Machines A and B were set to $P_A = 0.2$ and $P_B = 0.8$ for the first 50 plays, and were swapped in the next 50 plays, i.e. $P_A = 0.8$ and $P_B = 0.2$, in order to emulate a variable environment. In the experiment, 100 consecutive slot plays were performed, and this set of 100 cycles was repeated 10 times.

The green curve in [figure 6\(b, ii\)](#) shows the evolution of the accumulated team reward when polarization-entangled photons were used with HW_1 and HW_2 *aligned* ($\theta_{\text{HW}_2} = \theta_{\text{HW}_1}$). This reward reaches 93.4 after 100 plays, which is nearly the theoretical maximum, as demonstrated in [section 3.4](#).

We assumed that the greedy action was taken by Player 2 based on the polarization adaptation strategy employed in the single-photon decision-making method described in [sections 2.2](#) and [3.1](#) [9]. The orientation of the half-wave plate was controlled toward the higher-reward-probability slot machine by revising the polarization control (PC) value [7]. The PC value was limited to a maximum and minimum of 10 and -10 , respectively. Essentially, larger (positively large) and smaller (negatively

large) PC values indicate that the half-wave plate was rotated so that the polarization of the photon was toward the horizontal and vertical directions, respectively. (The details of the PC values are described in [Appendix B](#).)

The blue curve in [figure 8\(a\)](#) shows the evolution of the PC value of Player 2, which gradually approaches +10 in the first half and -10 in the second half. It indicates that Player 2 detected that Machine B was the higher-reward-probability machine in the beginning, and tuned his or her half-wave plate orientation toward the vertical, which corresponds to Machine B. After the 51st play, the half-wave plate approaches the horizontal (corresponding to Machine A) because Machine A dispenses more reward in the second half; thus, Player 2 indeed performed a *greedy* action with the intention of receiving a greater reward.

However, the reward accumulated by Player 2 does *not* exceed that of Player 1 throughout the slot machine play, as shown by the blue and red curves in [figure 8\(b\)](#). The conflict ratio increases over time due to the misalignment of the polarization bases ([figure 8\(c\)](#)). Furthermore, the team reward accumulated at cycle 100 is 77.1, which is significantly smaller than that in the previously discussed polarization-aligned optimal case; that is, the greedy action by Player 2 decreased the team reward as well as the individual rewards. [Figure 8\(d\)](#) summarizes the total reward at cycle 100 for Player 1, Player 2, and the team, the error bars indicating the maximum and minimum rewards. The preservation of equality between players and decrease of the team reward are clearly in agreement with the theoretical analysis results presented in [section 2.5](#).

4.2. Decision making in *correlated-photon*-based systems

While the casino setting was kept the same as in the case discussed in [section 4.1](#), orthogonally correlated photon pairs were subjected to the system to examine the greedy action performed by Player 2.

The orthogonally correlated input photon states were $\theta_1 = 45^\circ$ and $\theta_2 = 45^\circ + 90^\circ$, while HW₁ was configured with $\theta_{\text{HW}_1} = 0^\circ$. As shown previously in [figure 6\(a, ii\)](#), the expected reward probabilities of Players 1 and 2 were equal when HW₂ was aligned with HW₁ were aligned, namely, when $\theta_{\text{HW}_2} = 0^\circ$.

Player 2 then started performing greedy actions by applying the same PC updating strategy described above. The blue curve in [figure 9\(a\)](#) shows the evolution of the PC value (of Player 2), which gradually increases and approaches +10 in the first half, and then decreases and approaches -10 in the second half. These behaviours indicate that Player 2 detected that Machine B was the higher-reward-probability machine in the first half, but he found that Machine A was the higher-reward-probability machine after the 51st play. Indeed, the CDR increases, as clearly shown by the blue curve in [figure 9\(b\)](#). The CDR suddenly drops to zero after the 51st cycle due to the swapping of the reward probabilities of the slot machines; however, the CDR gradually returns to unity as time elapses. Consequently, the accumulated reward of Player 2 always surpasses that of Player 1, as depicted by the blue and red curves in [figure 9\(c\)](#). It is in a well agreement with the theoretical analysis presented

in [section 2.4](#). The conflict ratio shown in [figure 9\(d\)](#) always fluctuates and is large since Player 1 is effectively randomly choosing between the slot machines because $\theta_1 = 45^\circ$.

[Figure 9\(e\)](#) summarizes the accumulated rewards at cycle 100 with $\theta_1 = 45^\circ$ *without* greedy action by Player 2 ($\theta_{\text{HW}_1} = \theta_{\text{HW}_2} = 0^\circ$) and *with* greedy action by Player 2 in the assumed casino setting. Player 2 achieved deception through this greedy action, thereby destroying the equality. The consequences clearly differ between the correlated photon and polarization-entangled photon situations.

5. Autonomous polarization-basis alignment

As discussed above, polarization-basis alignment between the players is crucial to realize the maximal social benefits. Experimentally, this alignment was characterized by evaluating the photon pair statistics detected by APD1–APD4, as shown in [figure 4\(c\)](#), and showing that the coincidences were almost constant while rotating both wave plates, and that the signals of APD1 and APD3 were minimized, as were those of APD2 and APD4. However, the optical system may suffer from certain environmental disturbances during the decision-making operations that degrade its performance. Therefore, on-line calibration that does not interrupt the decision-making operation is important.

Such issues can be resolved by providing half-rewards to the players, because the receipt of a half-reward means that a conflict between decisions is induced and indicates the possibility of misalignment between the polarization bases. Here we discuss the resolution of these issues by two

different methods considering that the goal is to configure θ_{HW_2} with respect to the unknown θ_{HW_1} using an adaptation algorithm.

5.1. Assumption I: the sign of the polarization basis misalignment is known

First, it was assumed that the angle of the deviated half-wave plate angle, denoted by θ'_{HW_2} , was observable while the sign of the deviation with respect to the optimal angle, $\text{sign}(\theta'_{\text{HW}_2} - \theta_{\text{HW}_1})$, was known. The deviations of θ_{HW_2} and θ_{HW_1} were presumed *not* to be significant, typically less than 22.5° ; hence, slight recalibration was considered to be sufficient.

In the experiment whose results are shown by the blue curve in [figure 10\(a\)](#), θ_{HW_2} was *initially* 22.5° , and its deviation with respect to the optimal angle was *positive*, leading to $\theta_{\text{HW}_2} - \theta_{\text{HW}_1} > 0$. In fact, θ_{HW_1} was set to be 0° . Experimentally, we implemented realignment control by using the PC value; 22.5° corresponds to a PC value of +3. In this case, the realignment rule was to *decrease* the PC value by 1 if a half-reward event was observed. As demonstrated by the blue curve in [figure 10\(a\)](#), the PC value of Player 2 gradually approaches zero. It should be noted here that *identification* of the slot machine is *not* utilized in this method, which is a significant difference compared to the single-photon decision-making method [7, 8], and it is also used in the greedy action of Player 2. Indeed, the probability of conflict between decisions is given by $\sin^2 \left[2(\theta_{\text{HW}_1} - \theta_{\text{HW}_2}) \right]$ according to [equation \(21\)](#), indicating that θ_{HW_2} should be decreased to decrease the conflict between decisions. Note that the labels along the right-hand vertical axis of [figure 10\(a\)](#) are the corresponding actual half-wave plate

angles and not the PC values in order to facilitate intuitive understanding. The experimental details are provided in [Appendix E](#).

Similarly, when θ_{HW_2} was initially setup at -22.5° , deviating from the optimal angle by a *negative* amount, i.e. $\theta_{\text{HW}_2} - \theta_{\text{HW}_1} < 0$, the realignment strategy was to *increase* the PC value by 1 if a half-reward event was observed. As demonstrated by the brown curve in [figure 10\(a\)](#), the PC value increases and gradually approaches zero. The green curve represents the case in which the initial deviation was zero, meaning that the polarization bases were aligned. The accumulated reward evolution is almost the same regardless of the initial misalignment between the polarization bases ([figure 10\(b\)](#)). The conflict ratio decreases as the polarization bases become more aligned ([figure 10\(c\)](#)). Thus, autonomous polarization re-alignment was demonstrated.

5.2. Assumption II: no prior information about the polarization basis

The realignment strategy described above presumes that the deviation direction is observable, which is a rather strict condition. We investigated the possibility of aligning the polarization bases without any prior information, exploiting the fact that a half-reward event indicates conflict between decisions. Simultaneously, when the polarization bases are aligned, the probability of conflict between decisions, i.e. $\sin^2[2(\theta_{\text{HW}_1} - \theta_{\text{HW}_2})]$, is zero. Therefore, an alignment strategy is as follows.

[C-0] If the receipt of a half-reward is observed, update θ_{HW_2} by $\theta_{\text{HW}_2} + \Delta_a$.

Here, Δ_a is a constant employed to change θ_{HW_2} gradually. If Δ_a is sufficiently small, by repeating [C-0], the difference between the half-wave plate angles $\theta_{\text{HW}_1} - \theta_{\text{HW}_2}$ should eventually become small; hence, the probability of conflict between decisions should decrease.

In the experimental demonstration, θ_{HW_2} was initially -22.5° and Δ_a was 12.5° . θ_{HW_2} should be made equal to θ_{HW_1} , which was 0° . After setting the reward probabilities of Machines A and B, the same way as in the previous experiments, 100 consecutive plays were repeated 10 times. The evolution of θ_{HW_2} in each sequence is shown by the blue curves in figure 11(a), while the target angle $\theta_{\text{HW}_1} = 0^\circ$ is depicted by the red lines. After applying [C-0] twice, θ_{HW_2} was increased by $+25^\circ$; hence, θ_{HW_2} became 2.5° , which is sufficiently close to 0° . Even though θ_{HW_2} could not be exactly zero, it is evident from the evolution of θ_{HW_2} shown in figure 11(a) that θ_{HW_2} *passes through* the target angle and continues increasing. That is, even when $\theta_{\text{HW}_2} - \theta_{\text{HW}_1}$ is very small, conflict between decisions could not be perfectly avoided due to the imperfections of the experimental system (figure 4(c)).

5.3. Assumption III: no prior information about the polarization basis but memorization of conflict allowed

To prevent such escaping from the recalibrated angle due to error signals, one idea is to take the history into account. The revised calibration strategy is as follows.

[C-M] If conflicts between decisions have *not* been detected in the past M plays, the detection of conflict between decisions in the current play is *discarded*. If there were K occurrences of conflicts between decisions in the past M plays, *and* the current play yields a conflict between decisions, then

update θ_{HW_2} by $\theta_{\text{HW}_2} + \Delta_a$ and register the occurrence of a conflict between decisions in the memory of the M most recent plays.

In the experimental implementation, M and K were 5 and 1, respectively, which we call **[C-5]**, while $\Delta_a = 11.25^\circ$. As shown by the blue curves in [figure 11\(b\)](#), the half-wave plate angle successfully approached the target angle. With $\Delta_a = 11.25^\circ$, two position updates via **[C-M]** perfectly resolved the initially imposed misalignment (-22.5°), so that the effect of memorizing past events is clear.

Indeed, although it is rare, the case of [figure 11\(b, \(7\)\)](#) shows the half-wave plate angle still passing through the target angle. By more severely restricting the condition of rotating θ_{HW_2} by increasing M , the robustness against errors increases. As shown by the blue curves in [figure 11\(c\)](#) where M and K are 10 and 1, respectively, which is referred to as **[C-10]**, the event of passing through the target angle is avoided; however, the adaptation is very slow. Specifically, too large of a memory ($M = 10$, **[C-10]**) provides robustness against errors but results in very slow responses, whereas no memory ($M = 0$, **[C-0]**) yields a fast response but reactions that are too sensitive to error signals. A moderate parameter choice (**[C-5]**) resolves both the error tolerance and alignment speed issues. The green, red, and blue curves in [figure 11\(d\)](#) summarize the evolution of the accumulated team rewards based on the **[C-0]**, **[C-5]**, and **[C-10]** calibration rules, respectively, where **[C-5]** is optimal for maximizing the total team rewards.

6. Discussion

As demonstrated herein, entangled photons enable the achievement of maximum social rewards, equality among individuals, and prevention of selfish actions in communities when solving the CMAB problem. Clear differences between polarization-correlated and polarization-entangled photons were also observed.

If entangled photons turn out to be competitive in terms of social efficiency and equality, the *freedom* of decision of Players 1 and 2 is indeed completely ruled out by the strong authority imposed here by the specific probability properties of entangled states. In contrast, with two non-cooperative players using single photons, although the total team reward is very poor because of the conflicts between decisions, the *freedom* of choosing machines is fully guaranteed. A *mixture* of (i) social decision making by using an entangled-photon-based decision maker for efficiency and equality within a team, and (ii) individualistic decision making by using a conventional single-photon-based decision maker [6–9] for freedom, is an interesting and important topic for future study. Simultaneously, the conflict-avoidance nature of entangled photons may accelerate the exploration phase in finding higher-reward-probability selections among many alternatives, which is another topic requiring future research.

Likewise, another interesting topic [29] deals with the *modulation* of the degree of entanglement via HW_E and QW_E in the following form:

$$a|\theta_1, \theta_2\rangle + be^{i\phi}|\theta_2, \theta_1\rangle. \quad (26)$$

The parameters a , b , and ϕ are real numbers, so that an intended social metric is realized, rather than just maximally entangling the photons as was done in this study according to [equation \(7\)](#).

Finally, the scalability of entangled-photon-based decision makers is another fundamental topic in view of many practical applications. It is indeed technologically challenging to realize entanglement among many photons. The issue of scalability could be addressed by employing for example novel material systems [30–32] or integrated photonic circuits [33]. It could also be addressed by considering entangled photons combined with a certain coding strategy in order to process many bits of information in a time-multiplexed manner [8]. Hence, our pioneering results are anticipated to stimulate concrete implementation of entangled-photon (or more generally entangled-excitation)-based quantum decision makers.

7. Conclusion

We theoretically and experimentally demonstrated that entangled photons efficiently resolve the CMAB problem so that the total social reward is maximized and social equality is accomplished, while also preventing deceptive or greedy actions. In solving competitive two-armed bandit problems, two independent players using single-photon-based decision making found the higher-reward-probability machine, but the total reward was seriously decreased due to the conflicts of interest. Polarization-correlated photon pairs are useful, to some extent, for deriving non-conflicting decisions and obtaining a greater total reward, but they cannot eliminate conflicts between decisions perfectly. Moreover, this

method has difficulty to provide equality. In contrast, entangled photons both enable conflicts between decisions to be avoided and the theoretical maximum total reward to be obtained, while guaranteeing equality regardless of the common polarization basis shared by the two players. By highlighting the polarization-basis requirements for entangled photons, we investigated the issue of polarization and value alignment in decision making based on polarization-entangled photons. If polarization-entangled-photon-based decision making is employed, we demonstrated that deception or preventing the other player receiving a greater reward by performing greedy actions in the two-armed bandit problem, is impossible thanks to the physical properties of the polarization dependencies derived by quantum superposition of states. The reward is always equal among the players. Furthermore, the total social reward is decreased by greedy action in such a system. On the contrary, deception is achievable when the decisions are based on polarization-correlated photons. Autonomous alignment schemes based only on interest-conflict information were demonstrated.

The present work demonstrated that entangled photons are powerful resources for achieving social maximum benefits as well as addressing unique features such as preventing greedy actions when solving the CMAB problem. These features are the foundations of important applications, such as allocation of precious resources like energy or frequency bands in communication in the age of artificial intelligence.

Acknowledgements

This work was supported in part by the CREST project (JPMJCR17N2) funded by the Japan Science and Technology Agency, the Core-to-Core Program A. Advanced Research Networks and Grants-in-Aid for Scientific Research (A) (JP17H01277) funded by the Japan Society for the Promotion of Science and Agence Nationale de la Recherche, France, through the TWIN project (Grant No. ANR-14-CE26-0001-01-TWIN) and Placore project (Grant No. ANR-13-BS10-0007-PlaCoRe), the Université Grenoble Alpes, France, through the Chaire IUA award granted to G.B. and the one-month invited Professorship of M.N. We also acknowledge the Ph.D. grant to N.C. from the Laboratoire d'excellence LANEF in Grenoble (ANR-10-LABX-51-01).

Appendix A. Experimental system

A schematic diagram of the experimental setup is shown in [figure 2](#). A fiber-pigtailed, diode-pumped, solid-state laser (Obis, 405 FP) operated at a wavelength of 404 nm with an output power of 100 mW supplied excitation light through a quarter-wave plate (QW_E) (Thorlabs, WPQ05M-405) and half-wave plate (HW_E) (Thorlabs, WPH05M-405) into a PPKTP crystal (Raicol, type-II colinear SPDC cut) in a polarization Sagnac loop built by a polarization beam splitter (PBS_L) (OptoSigma, PBSW-12.7-3/7) and half-wave plate (HW_L) (Thorlabs, AHWP05M-600) [27]. The PPKTP crystal was mounted on a Peltier cooler (Raicol, Peltier controller) to hold the temperature at 313 K. The generated signal light was directed into the branch of Player 1 via a dichroic mirror (Thorlabs, BS011), while the idler light was sent to the branch of Player 2. Due to the limitations of the optical bench, 5-m-long optical fibers (Thorlabs, P1-780A-FC-5) were inserted for both branches, followed by half-wave plates (HW_1 and HW_2) (Thorlabs, WPH05M-808). In the single-player and two-non-cooperative-player cases,

polarizers (P^*) (Thorlabs, LPNIR050-MP2) were used. The signal and idler light were then separately subjected to a grating installed in a spectrometer (Roper Scientific, SP-2155 Monochromator) to obtain 805 nm and 812 nm light for the signal and idler, respectively. The signal light was incident upon PBS_1 (Thorlabs, PBS251) and detected by either APD1 or APD2 (Excelitas, SPCM-AQRH-16). The idler light went to PBS_2 (Thorlabs, PBS252) and was detected by either APD3 or APD4. The photon arrival time were evaluated using a 100-ps-bin-size multiple-event time digitizer (time-to-digital converter) (FAST ComTec, MCS6A), which was connected to a host computer (HP, Z400) with an Intel Xeon CPU (2.67 GHz), OS Windows 7 professional 64 bit. Three half-wave plates (HW_E , HW_1 , and HW_2) and a quarter-wave plate (QW_E) were mounted on motorized rotary positioners (Thorlabs, PRM1Z8) driven via DC servomotors and controlled by the host computer. LabVIEW (version 2012) was used to control the experimental system, including the slot machine emulation.

The slot machines were emulated in the host computer using pseudorandom numbers ranging from 0 to 1. If the random number was smaller than the reward probability of Machine A (P_A), a reward was dispensed. The same mechanism applied for Machine B.

Appendix B. Single-player and two-non-cooperative-player decision-making strategies

We describe the case when only Player 1 plays the slot machines. If in cycle t , the selected machine is Machine A and it yields a reward (in other words, if Player 1 wins by playing Machine A), then the polarization adjuster value of Player 1 (PA_1) is updated at cycle $t + 1$ according to

$$PA_1(t+1) = -\Delta_1 + \alpha_1 PA_1(t), \quad (27)$$

where α_1 is a forgetting parameter [7, 8] and Δ_1 is a constant increment. In this experiment, $\Delta_1 = 1$ and $\alpha_1 = 0.999$. The initial value of PA_1 is zero. If the selected machine (Machine A) does *not* yield a reward (i.e. if Player 1 loses), PA_1 is updated according to

$$PA_1(t+1) = +\Omega_1 + \alpha_1 PA_1(t), \quad (28)$$

where Ω_1 is a parameter that is adaptively configured concerning the history [8]. In this study, Ω_1 was a constant ($\Omega_1 = 1$), assuming the summation of the reward probabilities to be known ($P_A + P_B = 1$). Intuitively speaking, PA_1 *decreases* if Machine A is more likely to win and *increases* if Machine B is considered to be more likely to earn rewards. The value of PA_1 is then adapted to polarization control of HP₁. Specifically, the orientation of HP₁ at cycle t is determined by

$$HP_1(t) = \text{POS}_1(\lceil PA_1(t) \rceil), \quad (29)$$

where $\lceil \cdot \rceil$ represents the round-off function to the closest whole number. In the experiment, the rounded integer PA values were $-3, -2, -1, 0, 1, 2$, and 3 . When $PA_1(t) \geq 4$ or $PA_1(t) \leq -4$, the rounded PA value was defined by $\lceil PA_1(t) \rceil = 3$ and $\lceil PA_1(t) \rceil = -3$, respectively. The actual values of the orientations set according to [equation \(29\)](#) were determined by considering the asymmetry of the photon counts between APD1 and APD2, as discussed in the main article. Specifically, $\text{POS}(-3)$, $\text{POS}(-2)$, $\text{POS}(-1)$, $\text{POS}(0)$, $\text{POS}(1)$, $\text{POS}(2)$, and $\text{POS}(3)$ were given by -18.7° , -15.3° , -11.3° , 0° , 11.8° , 16° , and 21.2° , which are marked by the dotted lines in [figure 3\(a\)](#), so that the ratio of the photon

count by APD1 to that by APD2 was 20, 10, 5, 1, 1/5, 1/10, and 1/20, respectively, to resolve the asymmetry effectively. In addition, to prevent the PA value from being too large or too small, which could limit the speed of adaptation to environmental changes, the maximum and minimum PA values were set to 10 and -10 , respectively.

The adaptive decision making of Player 2 was implemented in the same way. The orientation of HW₂ was tuned differently to account for the sensitivities of APD3 and APD4. Specifically, POS(-3), POS(-2), POS(-1), POS(0), POS(1), POS(2), and POS(3) were -19.2° , -17.1° , -13.6° , 0° , 15° , 19.6° , and 21.5° , which are marked by the dotted lines in [figure 3\(b\)](#), so that the ratio of the photon count by APD3 to that by APD4 was 50, 30, 10, 1, 1/10, 1/30, and 1/50, respectively, to resolve the asymmetry effectively.

For a given slot machine play, the actual decision of Player 1 was made by the *identity* of the channel where the *first* photon arrival was measured [7]. If the first photon was detected by APD1, the decision was to select Machine A, whereas if it was detected by APD2, the decision was to choose Machine B. Likewise, the decision of Player 2 was made based on the first photon detection either by APD3 or APD4.

Appendix C. Implementation of collective decision making

Using the multiple-event time digitizer, four kinds of coincidence of observing photons at (i) APD1 and APD3, (ii) APD2 and APD3, (iii) APD1 and APD4, and (iv) APD2 and APD4 were measured.

For a given slot machine play, the *identity* of the *first* observation of the coincidence among the four possible combinations was considered to represent the decisions of Players 1 and 2. The correspondence between the photon measurement and the decision to be made was the same as in the abovementioned single-player cases; for example, measurement of a photon by APD1 corresponded to the decision of choosing Machine A for Player 1, while the detection of a photon by APD3 corresponded to the decision of choosing Machine A for Player 2. Therefore, for example, if the first coincident observation was made by APD1 and APD3, the decision of Player 1 was to choose Machine A, while that of Player 2 was also to choose Machine A.

The total rewards accomplished by correlated and entangled photon pairs presented in [figure 6](#) are the average accumulated rewards at cycle 100 when the polarization bases were 0° , 15° , 30° , and 45° . This was done to ensure fair comparison between the correlated and entangled photons concerning the contrasting behavior in the case of the correlated photons with polarization bases of 0° and 45° ([figure 6\(c\)](#)).

Appendix D. Definition of equality

The equality shown in [figures 6\(c, iii\)](#) and [6\(d, iii\)](#) was evaluated as follows. (1) Calculate the ratio between the average numbers of times that Players 1 and 2 selected the higher-reward-probability machine from the first play to the 50th play. (2) Calculate the ratio between the average numbers of times that Players 1 and 2 selected the higher-reward-probability machine from the 51st play to the

100th play. (3) Calculate the average of (1) and (2). This average is a reasonable metric regarding equality of the opportunities to select the higher-reward-probability machine taking into account the fact that the casino setting was different between the first 50 cycles and the next 50 cycles.

Appendix E. Implementation of autonomous polarization adjustment (Assumption I)

Autonomous polarization adjustment scheme I is similar to the greedy action of Player 2 described in [Appendix B](#) but differs in that the information about conflicts between decisions, rather than win/lose information, is used in this method. Specifically, the PC value of Player 2 is updated at cycle $t + 1$ according to

$$PC(t+1) = -\Delta + \alpha[PC(t) - PC(0)] \quad \text{if } PC(t) > R \quad (29)$$

and

$$PC(t+1) = \Delta + \alpha[PC(t) - PC(0)] \quad \text{if } PC(t) < R, \quad (30)$$

where R is the target or optimal value when the polarization bases are aligned, while α is the forgetting parameter, which is 0.999 as in the case of [equation \(27\)](#). The correspondence between the PC values and actual angles was the same as in the setup described in [Appendix B](#) (namely, the same as in the experiment on greedy action performed by Player 2). The PC values shown in [figure 10\(a\)](#) are the averages of the 10 repetitions of consecutive slot-machine playing; hence, due also to the forgetting parameter, the curves therein exhibit smooth time evolution.

References

1. Brunner D, Soriano M C, Mirasso C R, Fischer I 2013 *Nat. Commun.* **4** 1364
2. Inagaki T *et al* 2016 *Science* 10.1126/science.aah4243
3. Shen Y *et al* 2017 *Nat. Photon.* **11** 441.
4. Sutton R S and Barto A G 1998 *Reinforcement Learning: An Introduction* (Cambridge: The MIT Press)
5. Silver D *et al* 2017 *Nature* **550** 354
6. Naruse M *et al* 2014 *J. Appl. Phys.* **116** 154303
7. Naruse M *et al* 2015 *Sci. Rep.* **5** 13253
8. Naruse M *et al* 2016 *ACS Photonics* **3** 2505
9. Naruse M, Terashima Y, Uchida A, Kim S J 2017 *Sci. Rep.* **7** 8772
10. Horodecki R, Horodecki P, Horodecki M, Horodecki K 2009 *Rev. Mod. Phys.* **81** 865
11. Brukner Č, Pan J W, Simon C, Weihs G, Zeilinger A 2003 *Phys. Rev. A* **67** 034304
12. Dong D, Chen C, Li H, Tarn T J 2008 *IEEE Trans. Syst. Man Cyb. Part B* **38** 1207
13. Lai L, El Gamal H, Jiang H, Poor H V 2011 *IEEE Trans. Mobile Computing* **10** 239
14. Kim S J, Naruse M, Aono 2016 *Philosophies* **1** 245
15. Deneubourg J L, Goss S 1989 *Ethology Ecology & Evolution.* **1** 295
16. Franks N R, Dornhaus A, Fitzsimmons J P, Stevens M 2003 *Proc. Royal Soc. London B: Bio. Sci.* **270** 2457

17. Braess D, Nagurney A, Wakolbinger T 2005 *Transp. Sci.* **39** 446
18. Kuroda K, Kato H, Kim S J, Naruse M, Hasegawa M 2018 *Nonlin. Theor. Appl. IEICE* **9** 74
19. Kalai E, Lehrer E 1993 *Econometrica* **61** 1019
20. Reimer C 2015 *Nat. Commun.* **6** 8236
21. Eisert J, Wilkens M, Lewenstein, M 1999. *Phys. Rev. Lett.* **83** 3077
22. Prevedel R, Stefanov A, Walther P, Zeilinger A 2007 *New J. Phys.* **9** 205
23. Schmid C *et al* 2010 *New J. Phys.* **12** 063031
24. Zu C *et al* 2012 *New J. Phys.* **14** 033002
25. Nash J F 1950 *Proc. Natl. Acad. Sci.* **36** 48
26. Kwiat P G, Mattle K, Weinfurter H, Zeilinger A, Sergienko A V, Shih Y 1995 *Phys. Rev. Lett.* **75**
4337
27. Fedrizzi A, Herbst T, Poppe A, Jennewein T, Zeilinger A 2007 *Opt. Express* **15** 15377
28. Kok P *et al* 2007 *Rev. Mod. Phys.* **79** 135
29. Fedrizzi A, Škerlak B, Paterek T, De Almeida M P, White A G 2011 *New J. Phys.* **13** 053038
30. Sackett C A *et al* 2000 *Nature* **404** 256
31. Häffner H *et al* 2005 *Nature* **438** 643
32. DiCarlo L *et al* 2010 *Nature* **467** 574
33. Matthews J C 2009 *Nat. Photon.* **3**, 346

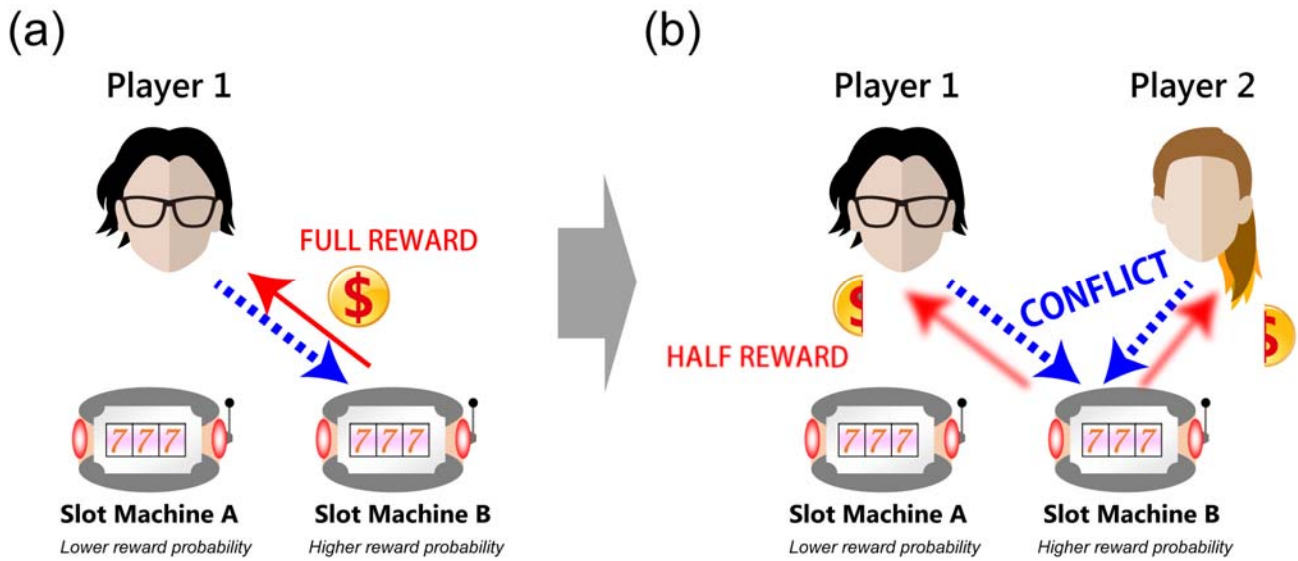


Figure 1. CMAB problem. (a) Two-armed bandit problem where a single player tries to maximize the total reward. When the player wins the machine, the *full* reward is supplied to the player. (b) Two players (Players 1 and 2) play the slot machines. Since both players want to choose the higher-reward-probability slot machine, conflicts are induced. In the case of conflict, the reward for each player is halved. If these two players are playing the casino as a *team*, such conflicts should be avoided to maximize the total reward as a team.

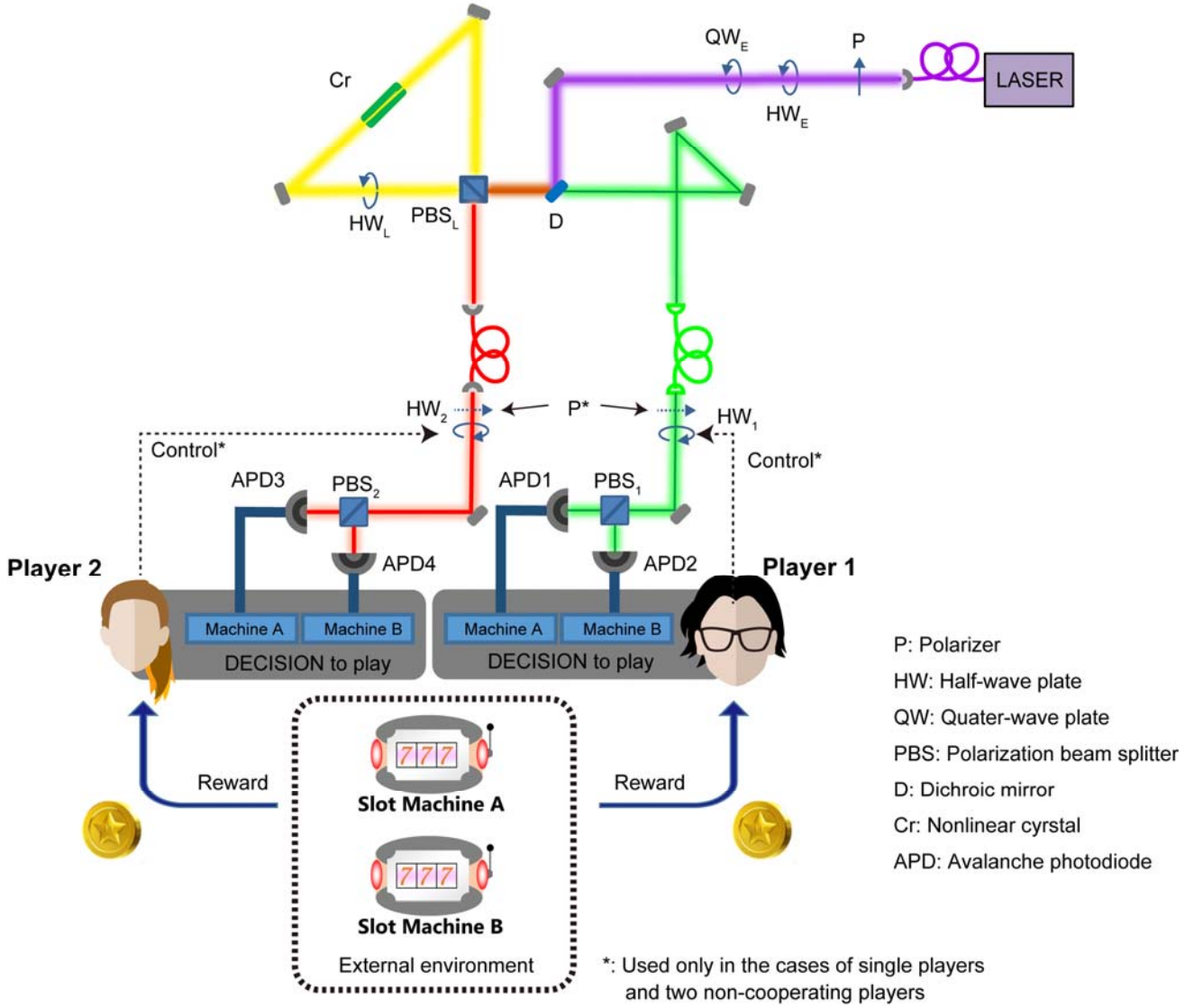


Figure 2. Experimental architecture for solving the CMAB problem using entangled photons.

Spontaneous parametric down-conversion is induced in a nonlinear PPKTP crystal inserted in a Sagnac interferometer architecture. The signal light is used for the decision of Player 1, while the idler light is used for that of Player 2 [27]. By configuring the half-wave and quarter-wave plates in front of the excitation laser, polarization-correlated or polarization-entangled photon pairs can be equally generated. The two slot machines (Machines A and B) are external environments, which are emulated in the host computer.

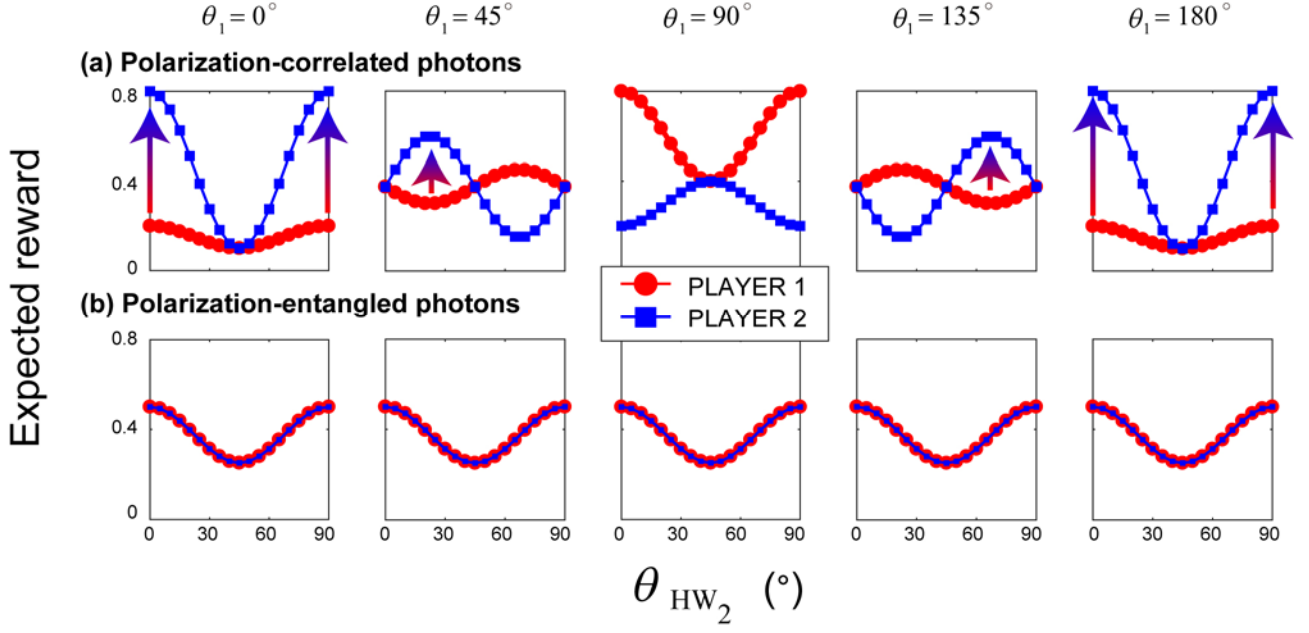


Figure 3. Expected reward when $P_A = 0.2$ and $P_B = 0.8$ and $\theta_{HW_1} = 0$. (i) With polarization-correlated photons, the expected reward could be biased toward a particular player. Also, no matter what the θ_1 is, the expected reward of a player can be greater than, or at least equal to, that of the other player; in other words, deception is possible. (ii) With polarization-entangled photons, the rewards are always equal to each other regardless of θ_1 and the misalignment of the polarization bases.

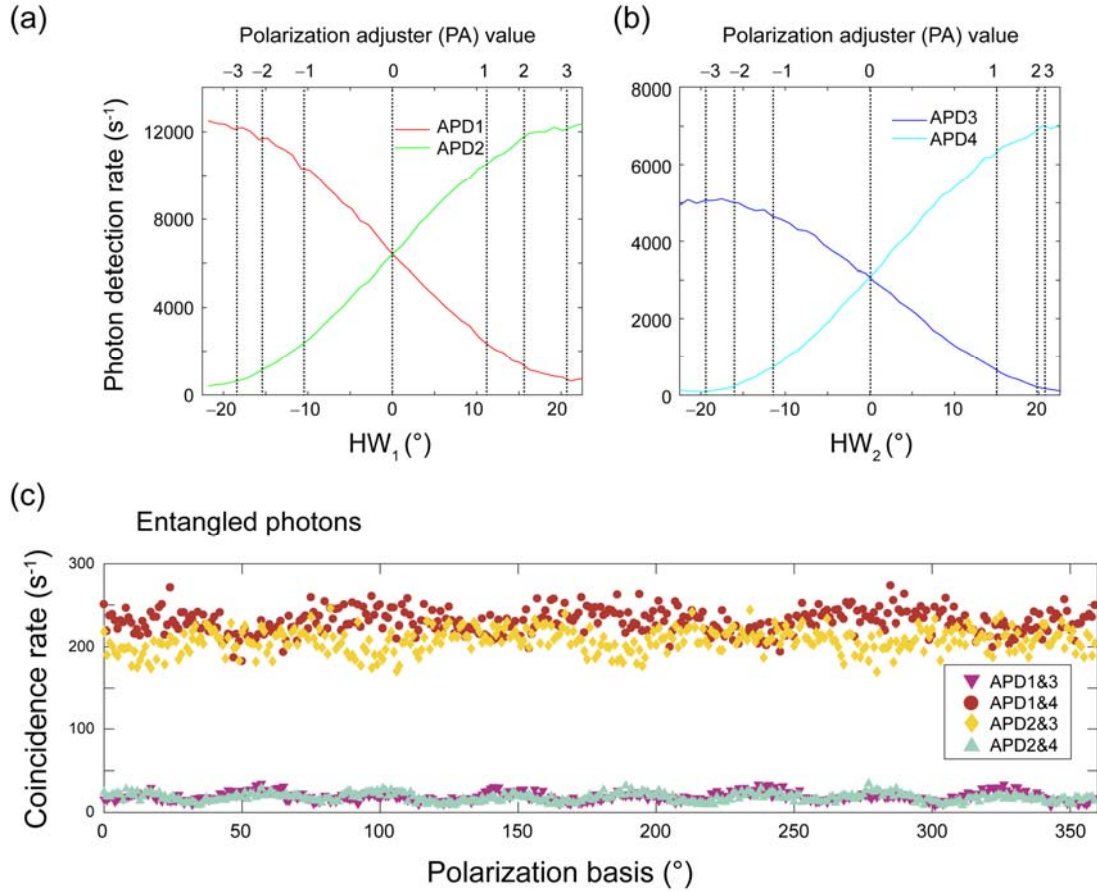


Figure 4. Characterization of the optical system. (a) With *non*-entangled photon generation and with the insertion of polarizers, the photon statistics related to Player 1 (APD1 and APD2) behave symmetrically (although not perfectly due to experimental imperfections) depending on the orientation of HW₁, which is located in front of PBS₁. (b) Similarly, the photon statistics related to Player 2 (APD3 and APD4) behave symmetrically depending on the orientation of HW₂, which is located in front of PBS₂. (c) Photon pair statistics when *entangled* photons are generated. Regardless of the common wave plate orientations (HW₁ and HW₂), consistent coincidence rates are observed along the polarization bases.

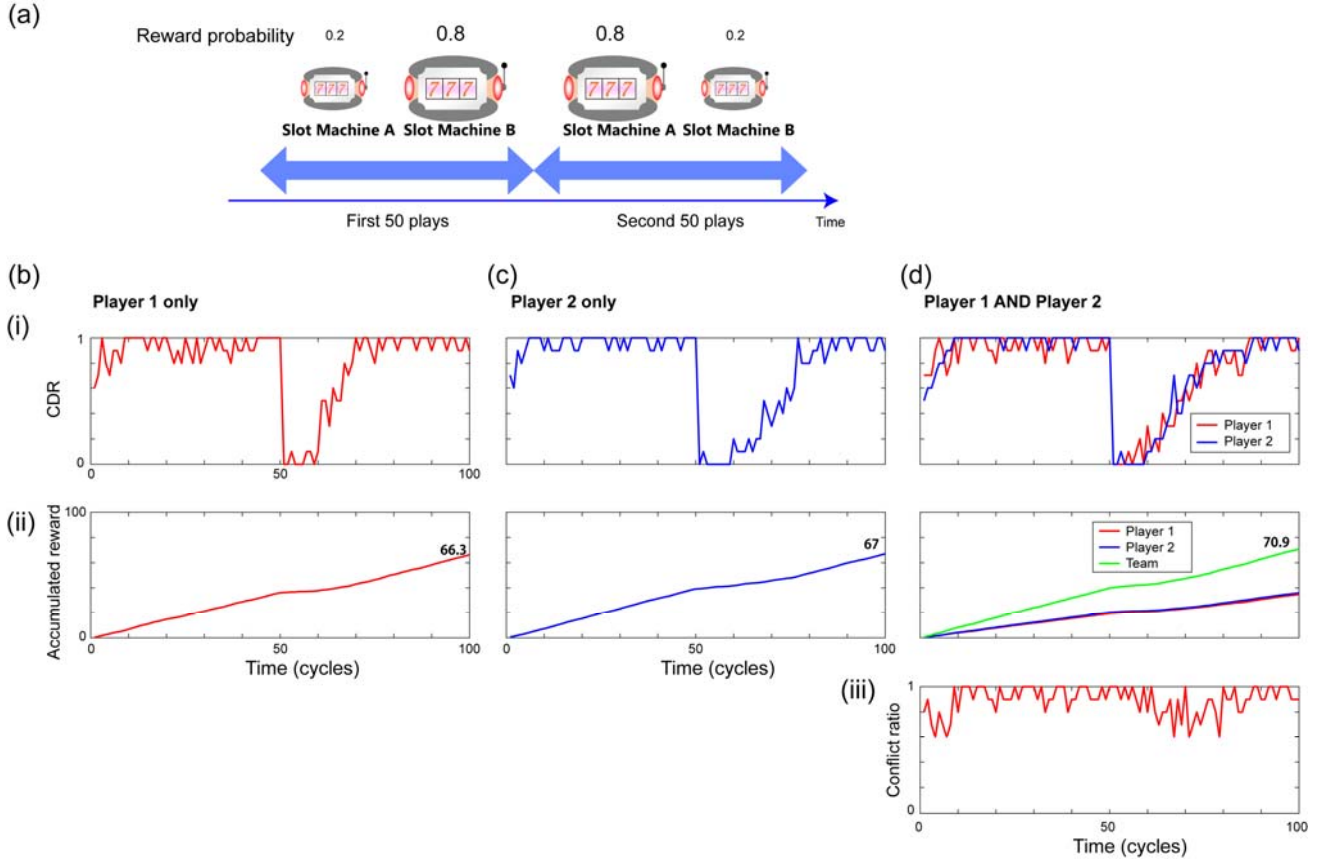


Figure 5. Decision making by a single player and two non-cooperative players. (a) Schematic illustration of the casino setting: the reward probability of Machine B is higher ($P_B = 0.8$) than that of Machine A ($P_A = 0.2$) in the first 50 plays, whereas that of Machine A is higher ($P_A = 0.8$) than that of Machine B ($P_B = 0.2$) in the second 50 plays. (b) Decision making when only Player 1 plays the casino. (i) The *CDR*, which is the ratio of choosing the higher-reward-probability slot machine over the number of trials, adaptively approaches unity, meaning that Player 1 is making *good* decisions. (ii) The *accumulated reward* linearly increases over time. (c) Decision making when only Player 2 plays the machines. (d) Decision making when both Players 1 and 2 play the machines. The CDRs of both players adaptively approach unity; that is, both players choose the higher-reward-probability machine. However, making the same decision causes conflict between their decisions, limiting the rewards for each of the players as well as the team rewards (ii). (iii) The *conflict ratio*, which is the ratio of the occurrence of identical decisions by the two players over the number of trials.

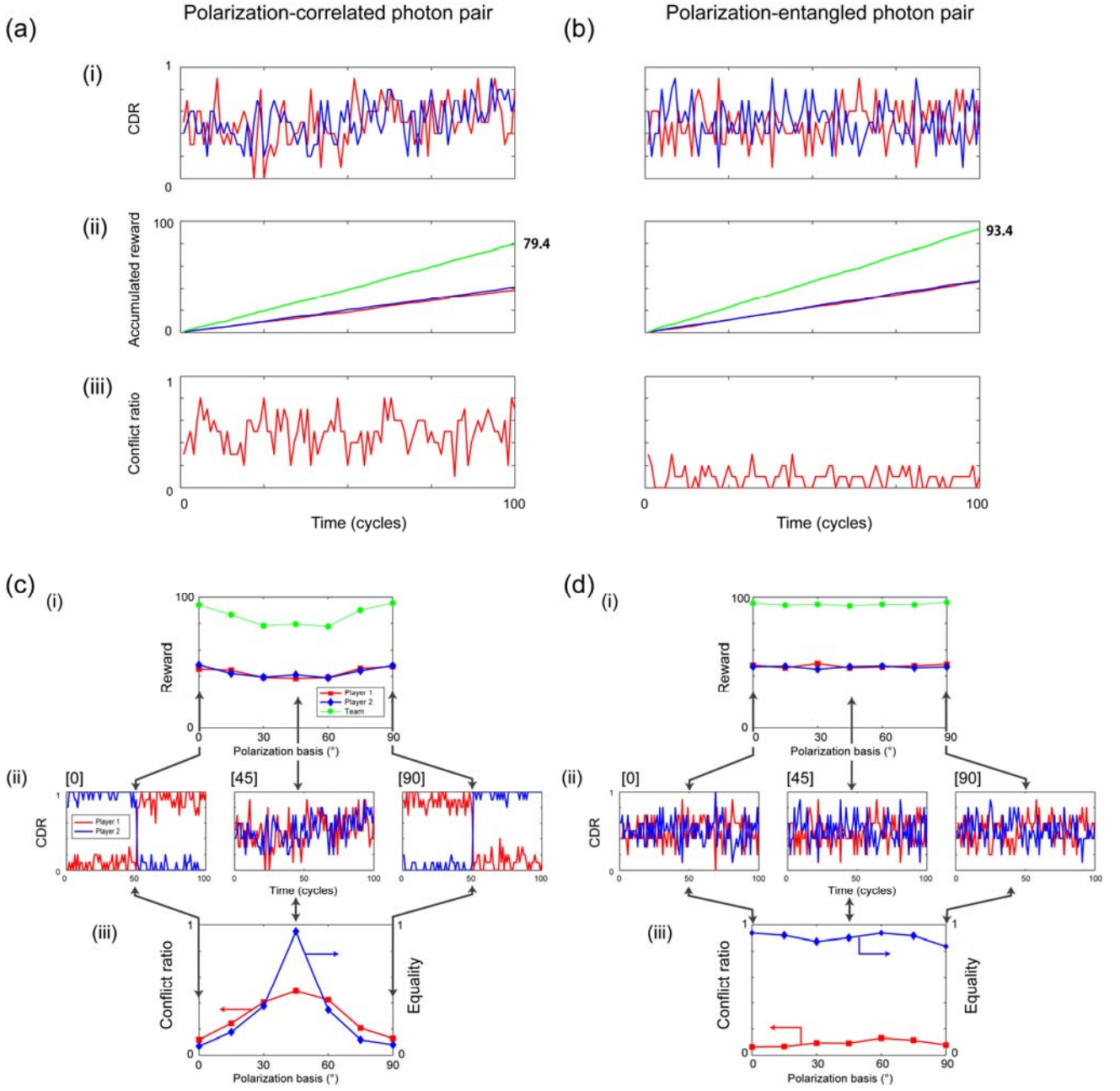


Figure 6. Collective decision making using polarization-correlated and polarization-entangled photon pairs. (a) With orthogonally polarized photon pairs, the total team reward improves. However, the conflict ratio is still large. (b) With entangled photons, the accumulated total team reward reaches the theoretical maximum and the conflict ratio is small. (c) Detailed analysis of the case of orthogonally polarized photon pairs. (d) Detailed analysis of the case of entangled photon pairs, where the low conflict ratio and high equality are preserved regardless of the polarization basis.

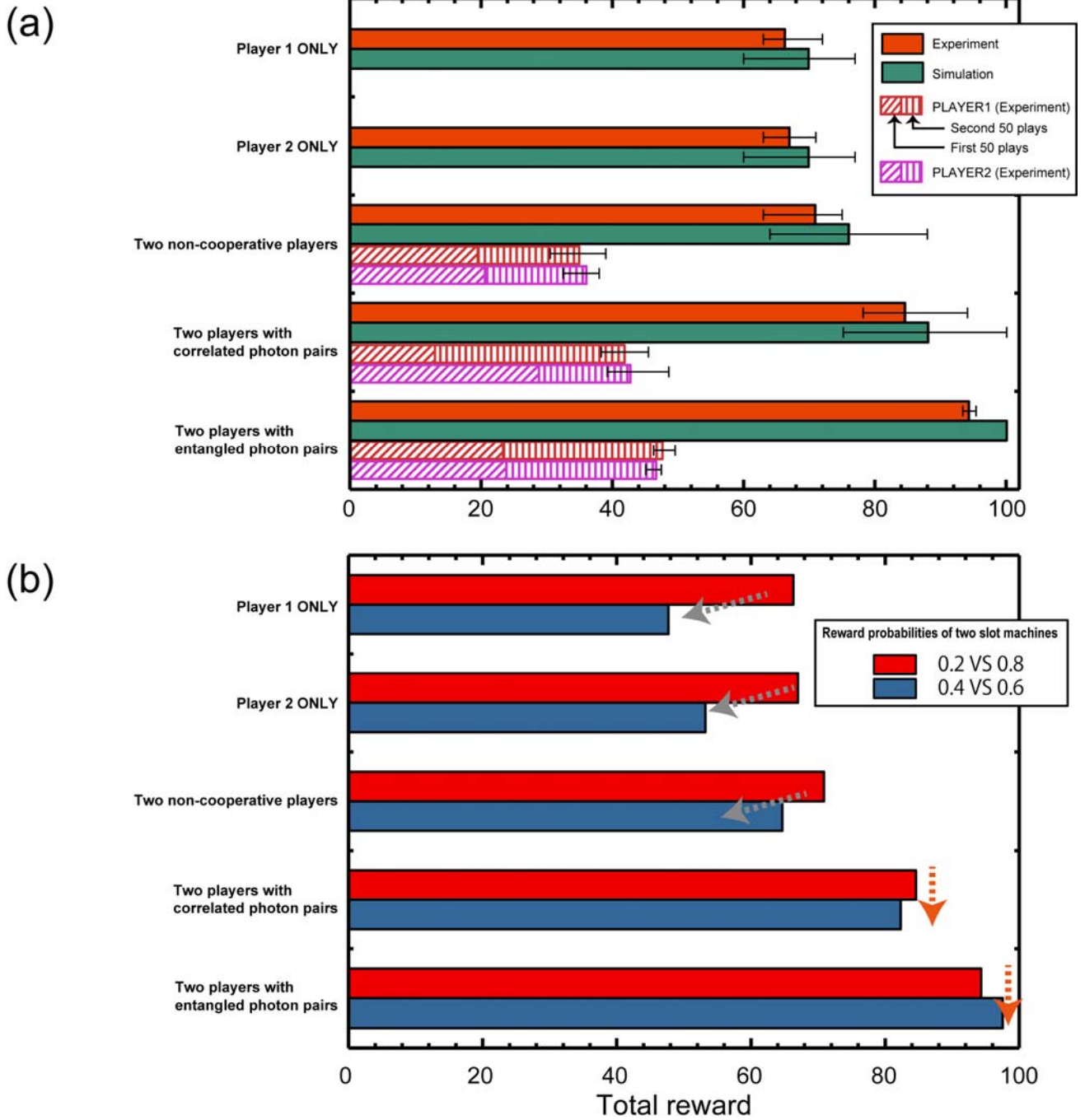


Figure 7. Comparison of total rewards in the cases of a single player, two non-cooperative players, and two players with polarization-correlated and entangled photon pairs and their dependencies on the decision difficulties. (a) Entangled photons provide the maximum team rewards. (b) As the difficulty of the given problem increases, the total rewards in the cases of single players and two non-cooperative players decrease whereas those in the cases of correlated and entangled photon pairs remain the same. The entangled photons provide the maximum rewards.

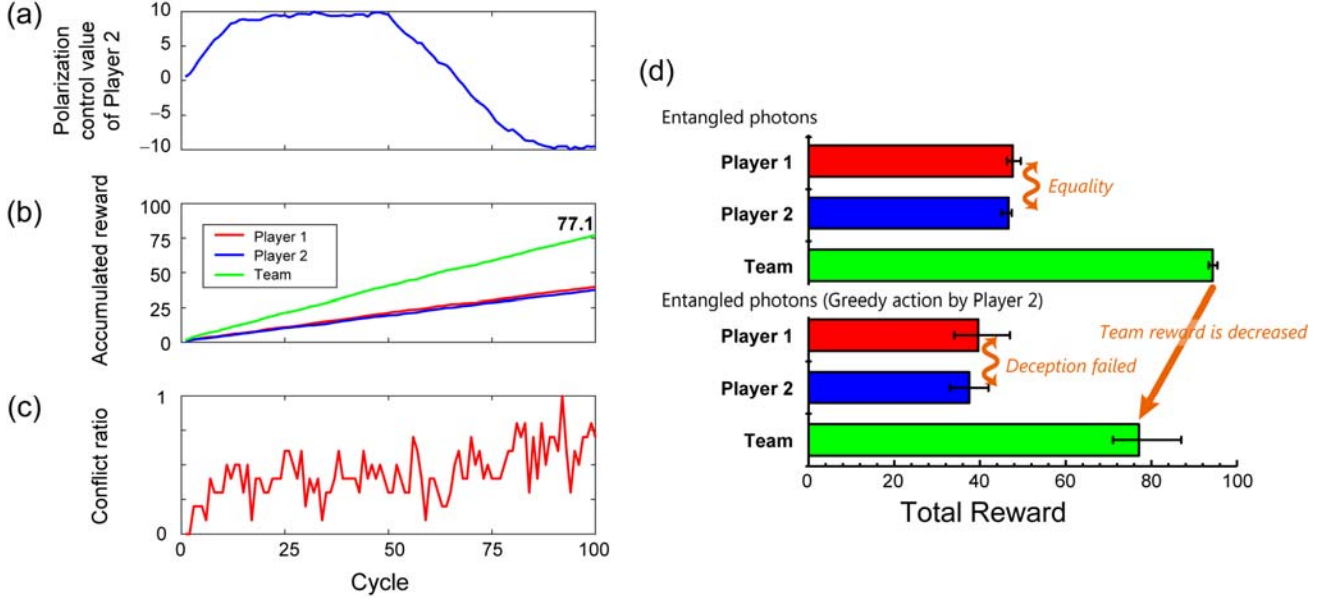


Figure 8. Prevention of deception or greedy action by polarization-entangled photons. (a) When Player 2 takes greedy actions, the half-wave plate is oriented toward the higher-reward-probability slot machine. (b) However, the accumulated reward of Player 2 is almost equal to that of Player 1, meaning that deception failed. Furthermore, total team reward is decreased. (c) The conflict ratio increases over time due to the misalignment of the polarization bases. (d) Accumulated rewards at cycle 100.

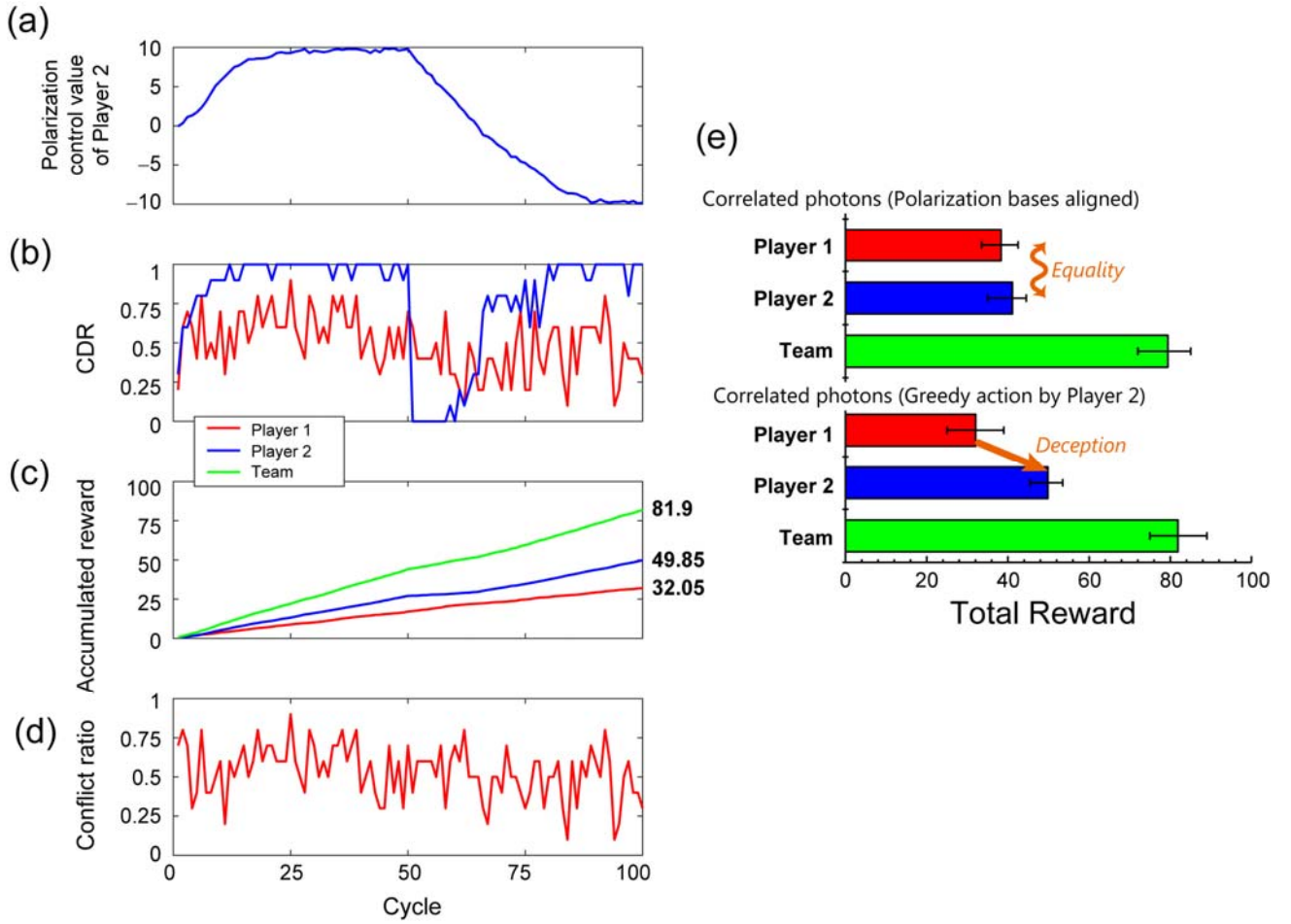


Figure 9. Deception is possible in correlated-photon-based systems. (a) The half-wave plate of Player 2 is gradually shifted toward the higher-reward-probability slot machine. (b) The CDR of Player 2 adaptively increases both in the first and second halves of the 100 cycles. (d) Consequently, the reward accumulated by Player 2 is greater than that of Player 1 although (e) the conflict ratio is high. (d) Accumulated rewards at cycle 100.

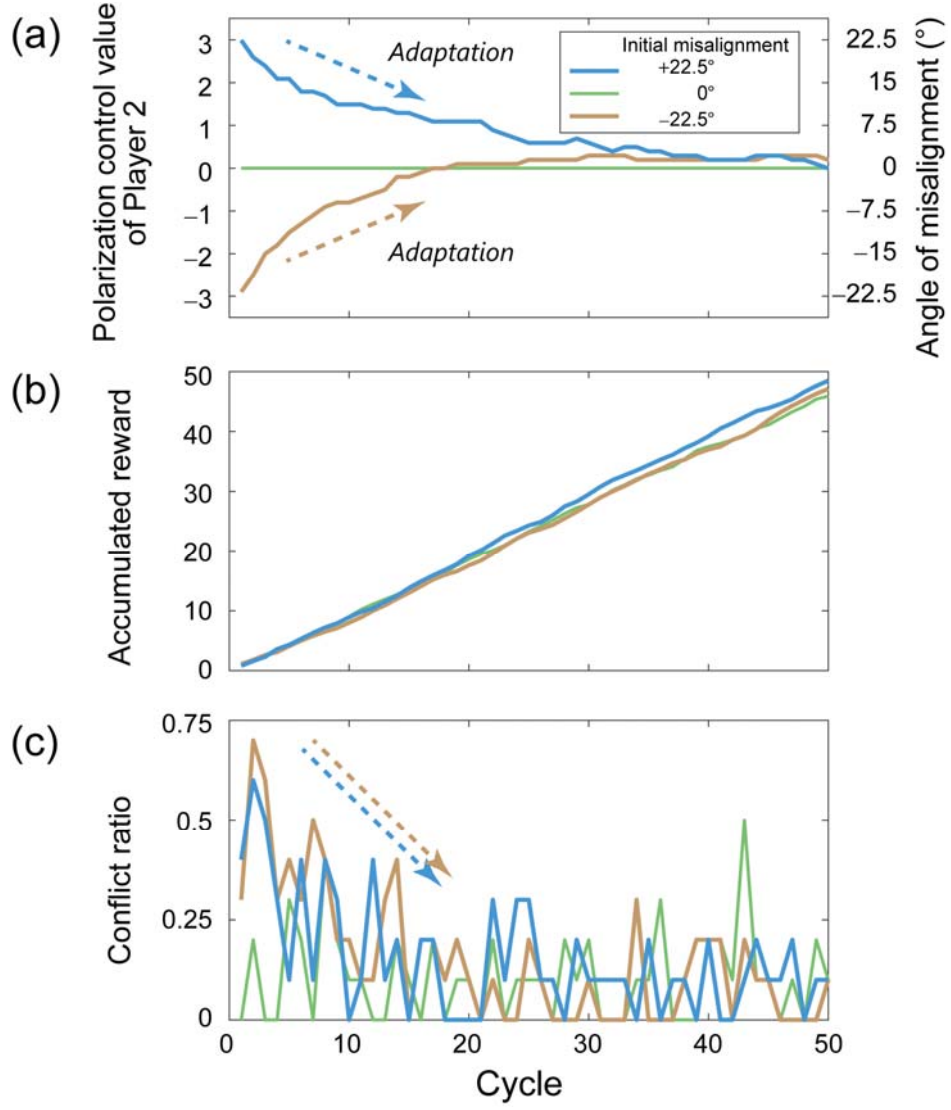


Figure 10. Autonomous polarization basis alignment under Assumption I. (a) Using the detection of conflicts between decisions and knowing the relative direction of deviation from the optimal situation, autonomous polarization basis alignment is accomplished. (b) The accumulated reward evolution is almost the same regardless of the initially induced misalignment between the polarization bases. (c) The conflict ratio decreases as the polarization bases become aligned.

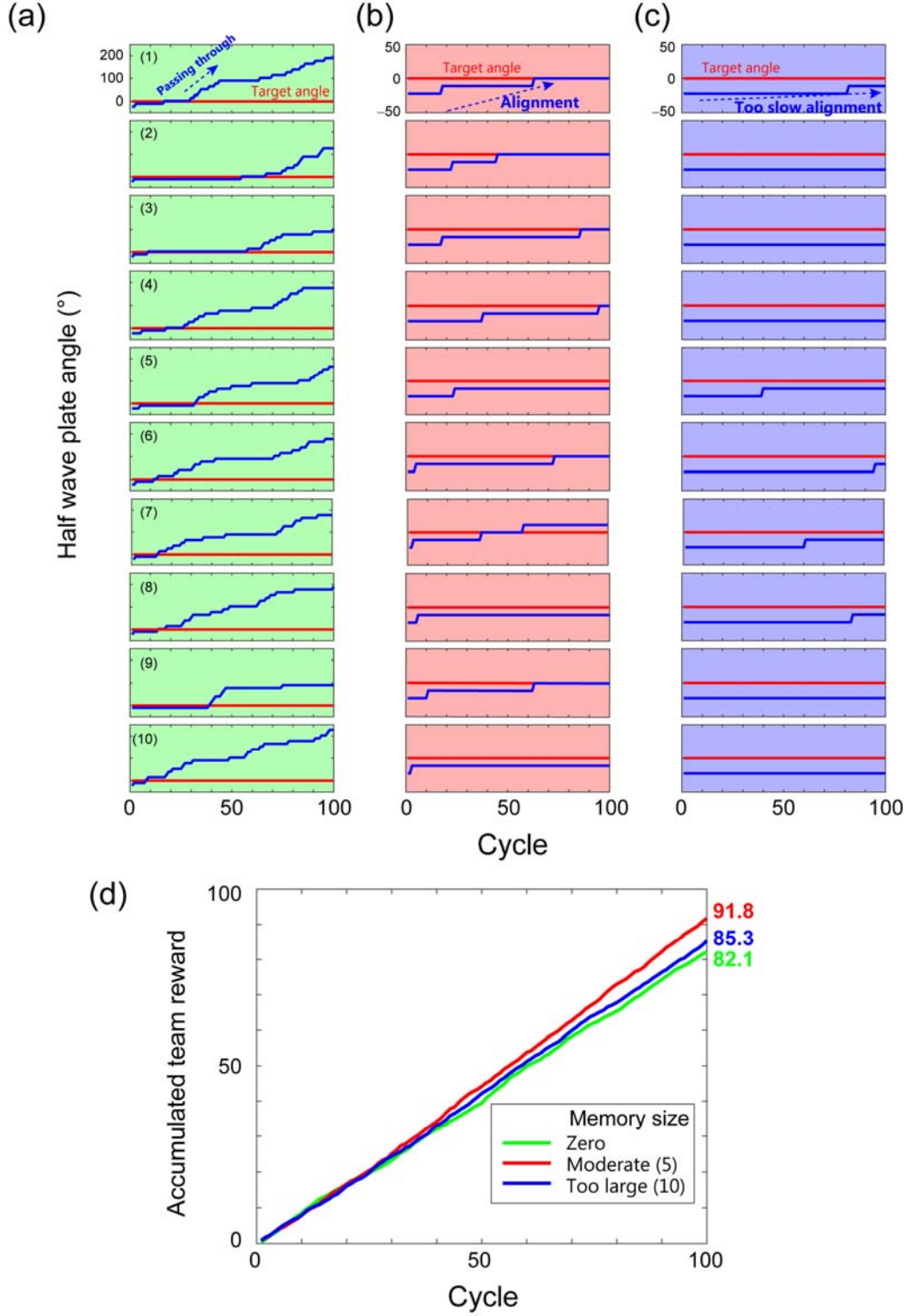


Figure 11. Autonomous polarization basis alignment under Assumptions II and III. Without any prior information, autonomous alignment should be possible by gradually rotating one of the half-wave plates. (a) However, due to the error signals that sometimes occur even when the polarization bases are aligned, the mechanism does not work well since the system *passes through* the optimal situation. (b) By referring to the recent history of the events involving decision conflict, robustness against errors is accomplished. (c) With too much reference to past events, the reaction becomes very slow.